Short Term Transient Pressure Tests - Design and Analysis Considerations

Jeffrey W. Knight, Halliburton Reservoir Services
Saeed Hedayati and James L. Hunt, Halliburton Services

ABSTRACT

Short term transient pressure tests can yield important hydrocarbon reservoir parameters including initial pressure, effective permeability, and dimensionless skin factor. These tests may be characterized by short time durations and limited areal investigation of the reservoir. They are often used to appraise new wells. Drillstem tests, closed-chamber drillstem tests, surge tests, and slug tests are all common short term transient pressure tests.

After a discussion of pressure analysis theory, this paper describes these tests in terms of procedure and information to be gained. Design factors are highlighted with emphasis on such practical points as recommended lengths of flow and shut-in periods, and ratio of shut-in time to flow time, when applicable. Some discourse on tools and data acquisition equipment required to perform each test from a conceptual viewpoint is provided in the following text. This paper also presents analysis methods for each test and demonstrates expected pressure responses with field and simulated data.

INTRODUCTION

Transient pressure tests yield valuable information when properly conducted and collected data are correctly analyzed. Questions are frequently asked concerning particular aspects of well testing operations such as "how long and how many times should the well be flowed and shut in?" Inquiries are often made as to the type of tools and pressure gauges that should be used in well testing. This paper is practical in nature and was designed for those with little or no previous experience in well testing while providing a refresher for those whose exposure to testing has been infrequent. It is hoped that the intended audience will gain increased understanding of the benefits of well testing and a working knowledge of common short term tests.

Short term tests have as primary objectives the determination of effective permeability, dimensionless skin factor, and initial pressure. These generally include drillstem tests (DST), closed chamber drillstem tests (CCDST), surge tests, and slug tests. Information provided by these tests often spares the operator subsequent expenditures should the tested zone prove disappointing. If the tested zone shows promise, valuable reservoir parameters are known which should prove beneficial in current evaluation and in future reservoir studies. Flowing a well and monitoring bottomhole pressure response provides a dynamic measurement of the well's productivity. Well testing makes sense economically when one considers the information that can be learned.

The remainder of the paper begins with an explanation of basic pressure transient theory which should clarify the necessity for gathering pressure/rate/time data. Thereafter, the four short term tests mentioned above will be described along the following lines:

- **I. Description and purpose**
- **II. Basic tools and instrumentation**
- **III. Design factors and simulated tests**
- **IV. Analysis methods and sample test.**

A few concluding remarks will follow.

BASIC PRESSURE TRANSIENT THEORY

In theory, all pressure transient testing involves upsetting the reservoir's equilibrium conditions and monitoring the reservoir's response to the disturbance. In practice, we disturb the reservoir by imposing a rate change on a well and then record downhole pressure response with a pressure gauge. An engineering model is required to relate pressure/rate/time performance at the well thus providing a basis to determine reservoir parameters. The foundation for pressure transient analysis of fluid-filled porous media is based upon the diffusivity equation:

$$\frac{\partial^2 p}{\partial r^2} + \frac{1}{r}\frac{\partial p}{\partial r} = \frac{\phi \mu c_t}{0.000264k}\frac{\partial p}{\partial t} \qquad (1)$$

This partial differential equation results from combining the continuity equation, Darcy's law, and an equation of state. With appropriate inner and outer boundary conditions and initial conditions, solutions to the diffusivity equation yield pressure as a function of both radial distance from the well and flow time. Inherent in the development of the diffusivity equation as presented in Eq. 1 are the following assumptions.[1-4]

1. Darcy's law applies
2. Single phase radial flow to the well
3. Constant reservoir thickness
4. Small pressure gradients
5. Negligible gravity effects
6. Homogeneous, isotropic reservoir
7. Isothermal behavior
8. Reservoir fluid has small and constant compressibility
9. Hydraulic diffusivity (η) is constant and independent of pressure,

$$where \quad \eta = \frac{0.000264k}{\phi \mu c_t}$$

For interested readers, references 5-8 provide a detailed look at the development of and solutions to the diffusivity equation. The particular solution of most interest in pressure transient analysis is derived by assuming the reservoir is infinitely large, the well is produced at constant rate, and pressure is equal throughout the reservoir before production commences. The prior three assumptions are the outer and inner boundary conditions and the initial condition, respectively. (See Fig. 1 for summary schematics highlighting the above assumptions.) The assumption of an infinitely large external radius, r_e, guarantees an infinite period of adjustment to the imposed disturbance or an infinite period of transient behavior. Obviously, no reservoir is of infinite extent; however, if production time is short, reservoir boundaries will likely not influence the pressure response. The tests to be described below generally involve short production times.

The E_i or line source solution[9] is an exact solution to Eq. 1 for the above stated assumptions and initial and boundary conditions:

$$p(r,t) = p_i + \frac{70.6\ qB\mu}{kh} E_i\ [-x\ ] \tag{2}$$

$$\textit{where the } E_i \textit{ function argument } x = \frac{948\phi\mu c_t\ r^2}{kt}$$

The above equation provides a functional relationship for pressure at any radial distance from the well, at any time, for a constant rate of production. From a practical standpoint, the desired pressure is the wellbore pressure, p_{wf}, since the pressure response is monitored at the wellbore during a well test. Inherent to the E_i solution is that the wellbore radius, r_w, is vanishingly small i.e., the wellbore can be considered a line, hence the term line source solution. At early times in a well test the measured wellbore flowing pressures will deviate from those predicted by Eq. 2 because the well is not a line. However, at practical times of interest, Eq. 2 is a suitable predictor of flowing wellbore pressure. The E_i solution is somewhat unwieldy and for values of the E_i argument $x < 0.02$ a natural log approximation[2] to the E_i solution may be used with very little error:

$$E_i\ (-x) = \ln\ (1.781x)\ \ for\ \ x < 0.02 \tag{3}$$

In order that the value of the E_i argument $x < 0.02$, t must be large and/or r must be small. Since pressure will be measured at a sufficiently small radius, r_w, and the test time will be large enough in all practical cases, the log approximation will apply. Substitution of the log approximation into Eq. 2 results in the following equation which predicts flowing bottomhole pressures in a well subject to the assumptions and conditions stated above:

$$p_{wf} = p_i - \frac{162.6qB\mu}{kh} \left[\log \left(\frac{kt}{\phi\mu c_t r_w^2}\right) - 3.23 \right] \tag{4}$$

Algebraic manipulation of Eq. 4 reveals that a plot of flowing wellbore pressure, p_{wf}, versus log of flowing time, t, is a straight line with the slope:

$$m = \frac{162.6\ qB\mu}{kh} \tag{5}$$

The slope of the line (see Fig. 2) is inversely related to reservoir transmissibility, kh/μ. If fluid viscosity, μ, and formation thickness, h, are known, permeability, k, may be calculated from

$$k = \frac{162.6\ qB\mu}{mh} \tag{6}$$

The permeability calculated from a well test is actually the effective permeability to either oil, gas, or water. Eq. 6 normally applies to liquid permeabilities.

The preceding developments constitute the classic semilog analysis for constant rate pressure drawdown in an infinite-acting radial flow reservoir system. Fig. 3 shows a comparison of three drawdowns, all with the same rate. The different semilog slopes are due to different permeabilities among the three cases.

During actual testing we find that early time data do not fall on a semilog straight line even as predicted by Eq. 4. The data deviate from a linear response due to the effects of wellbore storage.[10-12] In short, wellbore storage concerns unequal mass transfer. As long as the surface rate of production is not nearly equal to the sandface rate of production, wellbore storage exists and the pressure response is due to fluid movement within the wellbore. The true infinite-acting formation pressure response is masked until storage effects diminish. Calculations for reservoir parameters cannot be performed on this storage-dominated data using the classic semilog analysis. The pertinent problem with wellbore storage is one of recognition so the proper semilog data can be analyzed. Fig. 4 presents the effects of wellbore storage on the semilog analysis. Storage effects dominate the early portion of the upper curve. As storage effects decrease, this curve joins the linear trend of the curve not influenced by storage. Wellbore storage delays the appearance of analyzable semilog data.

Skin[10-15] is recognized as a region of either reduced or improved permeability around the wellbore. Drilling and completion operations are a prime source of reduced permeability at the sandface or wellbore damage, while some stimulation operations are an attempt to improve the near wellbore permeability or decrease the wellbore damage. The result of sandface skin damage is substantially reduced productivity. Fig. 5 presents three drawdown curves, all having the same rate and permeability, but with different skin factors. Lower flowing pressures and lower productivity result from higher skin factors. The following equation is used to calculate skin factor for a constant rate drawdown:

$$s = 1.151(\frac{p_i - p_{1hr}}{m} - \log \frac{k}{\phi \mu c_t r_w^2} + 3.32) \tag{7}$$

The variable p_{1hr} is the theoretical flowing pressure one hour into the drawdown test. This pressure must fall on the correct semilog straight line region.

Skin factors > 0 indicate wellbore damage while skin factors < 0 indicate flow improvement. A skin factor = 0 means an unaltered condition exists around the wellbore.

Type curves play a supporting role to, and sometimes serve as an alternative for, the pressure drawdown semilog analysis. These curves are simply solutions to the diffusivity equation, typically presented graphically on log-log coordinates. Dimensionless variables[4] are used so that a multitude of possible solutions can be shown on one graph. Type curve matching involves aligning a log-log plot of Δp, (p_i-p_{wf}) vs test time t for the actual test data over the type curve until a suitable match is found. Parameters such as permeability and skin may be determined from the matching process. Ref. 4 provides a description of the matching process.

Fig. 6 is a type curve for the E_i solution to the diffusivity equation. Use of this type curve will provide the same information as Eq. 2.

Ramey[10,11] presented the type curve shown in Fig. 7 for a single well in an infinite radial system, including wellbore storage and skin effects. The great utility of the graph is that it presents a means by which to analyze both early time and semilog data unlike the classic semilog method which cannot make use of the early data. For further understanding of the Ramey type curves, the defining equations[10,11] for the dimensionless variables are given below for dimensionless pressure

$$p_D = \frac{kh(p_i-p_{wf})}{141.2qB\mu} \tag{8}$$

dimensionless time

$$t_D = \frac{0.000264kt}{\phi\mu c_t r_w^2} \tag{9}$$

and dimensionless wellbore storage coefficient

$$C_D = \frac{5.615C}{2\pi\phi h c_t r_w^2} \tag{10}$$

$$where\ C = V_{wb}c_{wb}$$

The base case for this type curve is the curve for s = 0 and $C_D = 0$, which is the E_i solution. With the introduction of wellbore storage ($C_D > 0$), the type curves have a unit slope trend and then a transition, before joining the E_i solution. Thus, the type curve provides an indication of where the semilog data begin, or if any semilog data exist at all. The semilog region typically begins 1.5 log cycles[2] past the end of the wellbore storage unit slope line as illustrated in Fig. 8.

Note that as C_D increases (implying larger wellbore volumes and/or wellbore fluid compressibility) the onset of the semilog data is delayed to larger values of t_D. Also, as the dimensionless skin increases, p_D increases due to the effect skin has on lowering flowing pressures, as p_D is proportional to (p_i-p_{wf}). Present type curve technology incorporates different parameterization such as grouping C_D and s into one C_De^{2S} parameter[16] as well as the inclusion of pressure derivative.[17] Fig. 9 shows a type curve utilizing the newer features. Three items of interest are:

1. The pressure derivative has a unit slope which tracks the Δp curve during wellbore storage
2. For most values of C_De^{2S} the pressure derivative has a "hump" during the transition region between storage and infinite-acting behavior
3. For all values of C_De^{2S} the pressure derivative approaches a value of p_D=0.5, indicative of the infinite-acting radial flow or semilog region.

Although specifically developed for situations of pressure drawdown in liquid wells under the prior assumptions, the aforementioned type curves may be used to analyze pressure buildup data when the production time is large compared to the shut-in time. Agarwal's[18] equivalent time corrects the buildup time (Δt) such that the drawdown type curve may be used in cases where the production time is short or rate varies prior to well closure. As a rule of thumb, if the buildup time is greater than one tenth the prior production time, equivalent time should be used when curve matching. The buildup derivative log-log plot shape will be incorrect if the preceding drawdown was in storage.[18] The correct Δp for a buildup log-log plot is (p_{ws}-p_{wf}).

A few key assumptions pertaining to the formulation and solution of the diffusivity equation are violated with gas reservoirs. For example, gas fluid properties are a much stronger function of pressure, and gas compressibility is neither necessarily small nor constant. Gas pseudopressure[19] and pseudotime[20] are plotting functions which essentially correct gas well test data to fit the liquid well solutions of the diffusivity equation.

Gas pseudopressure takes into account the change in gas viscosity and gas compressibility factor with pressure

$$m(p) = 2 \int_{p_b}^{p} \frac{pdp}{\mu z} \tag{11}$$

Gas pseudopressure replaces pressure in semilog and log-log plotting of gas well test data.

Pseudotime takes into account variations with time of gas viscosity and total compressibility

$$t_a = \int_{t_o}^{t} \frac{dt}{\mu c_t} \tag{12}$$

Defined for buildup only, pseudotime replaces time in semilog and log-log plotting of gas well buildup data. Realistically, the best application for pseudotime is to correct storage-dominated gas well buildup data to the correct unit slope (constant C_D) line required by the previously discussed type curves. Gas wells may undergo large changes in compressibility during a buildup test, thus C_D changes, making type curve analysis difficult.

Several investigators[5,21,22] have proposed methods for analyzing pressure buildup data, with the method proposed by Horner[5] being the most popular one. Horner's equation for predicting the pressure buildup in a well following a single, constant rate period of production is:

$$p_{ws} = p_i - \frac{162.6 q B \mu}{kh} \log \left(\frac{t+\Delta t}{\Delta t}\right) \tag{13}$$

Eq. 13 implies that a plot of bottomhole shut-in pressure versus log of dimensionless Horner time, $(t+\Delta t)/\Delta t)$ is a straight line, with the slope inversely related to transmissibility. Effective permeability is calculated from the slope in the same manner described for the drawdown analysis (Fig. 10).

Horner analysis allows an extrapolation of the transient pressure response to infinite shut-in time (as $\Delta t \rightarrow \infty$, $(t+\Delta t)/\Delta t \rightarrow 1$) to obtain an extrapolated pressure, p*. For a new well in a large reservoir that has experienced limited production, p* should be equal to the initial pressure, p_i. Skin may be calculated from pressure buildup data with the following equation:

$$s = 1.151 \left(\frac{p_{1hr} - p_{wf}}{m} - \log \frac{k}{\phi \mu c_t r_w^2} + 3.23\right) \tag{14}$$

The variable p_{1hr} is the theoretical shut-in pressure one hour into the buildup test. This pressure must fall on the correct semilog straight line region.

Fig. 11 displays three buildup curves with different slopes due to different permeabilities only. Wellbore storage can affect pressure buildup also, and Fig. 12 shows the delay of semilog data on one curve because of wellbore storage effects.

It should be noted that the Horner method assumes one constant rate of production prior to well closure. In practice this is difficult to achieve, and hence, rigorous use of superposition[4] for a varying rate schedule may be necessary. Superposition is a mathematical principle associated with partial differential equations of the type as the diffusivity equation. Practically, it allows a solution to be formulated for a well's pressure behavior given any prior rate history. The Horner[5] and Miller et al.[22] methods utilize superposition considering one constant rate prior to well closure.

The flow period preceding well closure is very important because it establishes a pressure drop or gradient away from the well. If pressure around the well is not appreciably reduced by the drawdown, no meaningful pressure buildup will occur.

The maximum information gained during a well test comes from transient data[23], including effective permeability, skin factor, and p* (for buildups). The short term tests described below involve the collection of transient data; however, the analysis methods will not necessarily be limited to the above described semilog techniques. It is interesting to note that whatever the analysis method, the fundamental basis is the diffusivity equation. Usually, modifications to inner boundary conditions produce different analysis techniques.

Although the necessity of pressure/rate/time data has been emphasized, fluid property data is no less important in obtaining good pressure transient analysis results. In many exploratory wells, fluid properties will not be known at the time of the test and therefore, correlations must be used which will not present a problem in short term tests since in many instances an operator may only require ballpark values for further decision making.

DRILLSTEM TEST (DST)

I. Description and Purpose

The DST is a frequently run short term test, introduced to the industry in 1926.[24] An arrangement of tools and valves are carried to the bottom of the well on the drillstring to allow a zone of interest to be isolated and selectively flowed and closed-in. DSTs are performed on wildcat wells, offsets, and on infill wells. Upon successful completion of a DST and analysis of the collected data, an operator should have a basis for decisions concerning further expenditures on the zone. Typical information that DSTs can provide include effective permeability, skin factor, initial pressure, and fluid type present in the formation. In summation, the DST provides a temporary completion of a well so that a transient pressure test may be performed and valuable information collected with minimal expenditures. A pressure/time trace of a common DST is shown in Fig. 13.

II. Basic Tools and Instrumentation

DSTs may be run in open or cased hole and there exist several variations of tool strings that are utilized depending upon operator requirements. Conceptually, all DSTs are similar and the following five components[25] are necessary:

1. **Drillstring** - carries the DST tools downhole and serves as a conduit for produced fluids
2. **Packer** - isolates the zone of interest and relieves the formation of the hydrostatic overbalance due to the drilling or completion fluid thus allowing formation flow
3. **Perforated pipe** - provides a path through which fluids may flow from the reservoir into the drillstring
4. **Test valve** - provides the means to allow the reservoir to flow or to close-in as needed
5. **Pressure gauge** - provides a pressure record of the test and a crosscheck when difficulties are experienced

It is a good practice to run at least two pressure gauges to allow for comparison if problems are encountered during the test. One gauge is usually run "blanked-off" at the bottom of the test string. This gauge is not in the direct path of the fluid flow but senses pressure changes in the annular region. The other gauge is placed "in-stream," i.e., in the direct flow path, usually above the packer. Gauges should be properly sized "pressure-wise" according to the maximum expected pressures during the test (including hydrostatic and reverse-out pressures) as well as "time-wise" according to the total planned test time (including tripping in and out of the hole). In the U.S., a majority of DSTs employ mechanical pressure gauges although service companies now offer electronic memory recorders for use in DST strings. A cased hole DST will have nearly all the pressure recorders in a single bundle carrier.

Strictly speaking, the DST described here is run with an open surface valve. Many liquid wells will not flow to the surface during the allotted production time on a typical open hole DST. On such wells, the flow period should actually be called a slug period or a period in which there is an increasing bottomhole pressure due to the increasing hydrostatic pressure exerted by the liquid as the pipe fills up. On liquid wells that exhibit slug flow, the rate will be determined based on the pressure data or on the reported liquid recovery in feet, or in barrels if the recovery is reversed out to a tank. Gas wells often flow at the surface and rate may be determined based on surface conditions. A DST well configuration schematic is presented in Fig. 14.

III. Design Factors and Simulated Tests

For DSTs, two flow and closed-in sequences are recommended as a minimum since comparison of the initial and final closed-in extrapolated pressures serves as a check for possible depletion. The first flow period should be long enough to bleed off excess pressure (supercharge) caused by overbalanced drilling. If this excess pressure is not bled off, the initial first closed-in pressure may build to a pressure greater than formation pressure. Supercharge is more likely to be seen in oil well testing than gas testing due to the high compressibility of gas. Supercharge effects are also more likely seen in low to medium permeability zones than in highly permeable zones. Regardless of the type of fluid present or the formation permeability, there are compelling reasons to flow most wells at least 30 minutes upon initial opening. These include:

1. More likely to relieve supercharge, if present;
2. More likely to clean up some of the wellbore damage and return the well to its natural productivity, and
3. More likely to lift the rathole volume of mud above the test valve.

The initial buildup should be twice the length of the initial flow as a minimum, to allow for an accurate extrapolated pressure. The purpose of the second flow period is to draw the reservoir pressure down a considerable distance from the wellbore, setting up a good final buildup.

Ideally, the flow rate will stabilize so that an accurate rate may be determined. It is best to allow the surface indications during the second flow period to guide the duration of the final flow and closed-in sequence. For example, a strong surface "blow" during the final flow period indicates good productivity, and, thus, a one hour flow is probably sufficient. The final buildup should be at least as long as the final flow, while a buildup of 1.5 to 2 times the flow duration provides a more confident pressure extrapolation.

For weak surface action, a longer flow time is necessary to adequately investigate out into the reservoir. The final buildup should then be at least twice the flow time and possibly 2.5 to 3 times the flow period to better insure the probability of obtaining good semilog data. For an accurate pressure extrapolation, the correct infinite-acting portion of the data must exist. Should the blow begin to die during the second flow period, the final buildup should be initiated immediately or else the well may kill itself due to hydrostatic backpressure. If that occurs, there will be no final buildup.

It is important to realize that the maximum time on bottom for an open hole DST is about 4 to 6 hours. This limitation should be considered when planning test flow and closed-in times.

The above guidelines are a combination of previous suggestions[1-4] and experience. It should be noted that many times, valuable qualitative information may be gained from a test, even when no quantitative analysis is possible. For instance this may be due to a lack of pressure development during the buildups, or lack of a measurable hydrocarbon rate.

Figs. 15 to 17 present theoretical responses for various one flow/one closed-in oil producing DSTs. (All theoretical responses in this paper were generated with a well test simulator.[37]) In Fig. 15 the hydrostatic pressure builds up much more quickly during the slug flow period for the high permeability case. The pressure buildup occurs much more quickly for the high permeability case also. Skin damage will inhibit the productivity; e.g., in Fig. 16 notice the slower pressure increase due to the slower rate of liquid influx into the pipe for the damaged case. However, the buildup occurs more rapidly for the damaged case. Fig. 17 presents differences in behavior for a low permeability case for different skin factors.

IV. Analysis Methods and Sample Tests

DST flow period bottomhole pressure data are rarely analyzable by the previously discussed semilog method. For gas zones, the rate seldom stabilizes in the short time allotted for production. Therefore, gas well DST flow period bottomhole pressures are not frequently analyzed; however, surface pressures are used in conjunction with surface equipment to determine gas rate for buildup analysis. Semilog methods are preferred in the analysis of DST pressure buildup data as long as semilog data exist.

The first field case presented in this paper is an oil zone DST. The pressure/time representation of the two flow/two closed-in period test is shown in Fig. 18. Estimated rock and fluid data and other pertinent test data are presented in Table 1. Raw pressure/time data are given in Table 2. Initial and final buildup period processed data are given in Tables 3 and 4 respectively; results are summarized in Table 5. The steps below explain the analysis procedure.

1. A log-log plot (Fig. 19) of both closed-in periods indicates that only the second buildup period data reach the appropriate semilog region. The Horner plot (Fig. 20) confirms that the second buildup period data have a linear character at late time. The second buildup is analyzed for effective permeability, skin, and extrapolated pressure. Any attempt at semilog analysis of the first buildup will result in incorrect parameters because the correct semilog slope has not developed.

2. A rate must be determined from the slug flow period. Fig. 21 is an enlarged view of the pressure response during the flow periods. The rate of pressure change with time ($\Delta p/\Delta t$) is nearly constant and the slope of the second flow period pressure/time response can be used with the following equation to determine rate:

$$q = 2.0736 \times 10^5 (\frac{\Delta p}{\Delta t}) \frac{V_u}{\rho} \tag{15}$$

q = 2.0736 x 10^5(0.9)(0.00492)/(48.8)
q = 18.8 bbls/day

The recovery method is a possible alternative to the above pressure change method. The recovery method requires the known amount of liquid recovery above the test valve and the size(s) of pipe filled with the recovered liquid. A volume of recovery can then be calculated and a rate for the test determined based on the total flow time.

3. The semilog slope on the expanded Horner plot (Fig. 22) can be determined by subtracting the pressure at log cycle 1 from the pressure at log cycle 0, (same as p*).

$$m = |p^* - p_1| \tag{16}$$

$$m = |2546.9 - 2432.3| = 114.6 \text{ psi/cycle}$$

4. To calculate permeability

$$k = \frac{162.6\, q B \mu}{mh}$$

$$k = \frac{162.6(18.8)(1.545)(0.33)}{114.6(12)} = 1.13\ md$$

5. To calculate skin the following modified skin equation for short producing time is used

$$s = 1.151[\frac{p^* - p_{wf}}{m} - \log(\frac{kt}{\phi \mu c_t r_w^2}) + 3.23] \tag{17}$$

$$s = 1.151[\frac{2546.9-128.6}{114.6} - \log(\frac{1.13(1.523)}{0.10(0.33)(22.91 x 10^{-6})(0.345)^2}) + 3.23]$$

$$s = +19.6$$

The next case presented is a gas zone DST. The pressure/time representation of the test is presented in Fig. 23. Estimated rock and fluid data and other test information are given in Table 6. Pressure time and data are presented in Table 7. Initial and fixed buildup period processed data are given in

Tables 8 and 9, respectively. Results are summarized in Table 10. The steps below explain the analysis.

1. A log-log plot utilizing real gas pseudopressure (Fig. 24) indicates the second closed-in period data reached the correct semilog region. The Horner plot, also with pseudopressure, (Fig. 25) shows the semilog response straightening during the second buildup.
2. To calculate rate use the reported stabilized surface pressure of 25 psig on a 0.25 in. positive choke during the second flow. A suitable field determination of gas flow rate can be made with the following equation for 6-inch positive chokes.

$$q = \frac{Cp}{\sqrt{\gamma T}} \tag{18}$$

$$q = \frac{26.51(25+14.65)}{\sqrt{0.6(80+460)}} = 58 Mscf/D$$

3. From the expanded Horner plot (Fig. 26), we determine a suitable semilog line and calculate the slope as

$$m = |m(p^*) - m(p_1)| \tag{19}$$

$$m = |1037.5 - 966.7| = 70.8 \text{ MMpsi}^2\text{/cp/cycle}$$

4. To calculate permeability

$$k = \frac{0.001637\ qT}{mh} \tag{20}$$

$$k = \frac{0.001637(58)(180+460)}{70.8(10)} = 0.086\ md$$

4. To calculate skin the short producing time equation yields

$$s = +13.2$$

$$s = 1.151[\frac{m(p*) - m(p_{wf})}{m} - \log(\frac{kt}{\phi \mu c_t r_w^2}) + 3.23] \tag{21}$$

$$s = 1.151[\frac{1037.5\ -\ 0.3818}{70.8} - \log \frac{0.086(1.305)}{(0.10)(0.022)(148.9\,x\,10^{-6})(0.365)^2} + 3.23]$$

CLOSED CHAMBER DRILLSTEM TEST (CCDST)

I. Description and Purpose

Alexander[26] proposed this modified version of the DST in 1977. While similar to the conventional DST, the closed-chamber DST utilizes a closed surface valve during the flow periods. Rigorous use of surface pressure changes (dp/dt) and liquid influx data allow calculation of gas and liquid rates. Normal analysis of pressure buildup data taken during the closed-in periods may proceed with the known rates. According to Alexander CCDST offers greater security and safety over a standard DST and the rates can be used to estimate flow times necessary for fluid recovery in order to design surface equipment for future conventional testing.

CCDST appears particularly suited to low permeability gas well testing. The test provides permeability, reservoir pressure, skin, and a fluid sample. A bottomhole pressure/time trace of a common CCDST may resemble that of DST (See Fig. 13.).

II. Basic Tools and Instrumentation

The tools and instrumentation required for CCDST[26] do not significantly differ from those required for DST. Note that the additional hardware required over a conventional DST include:

1. A continuous recording surface pressure gauge from which surface pressure change with time (dp/dt) may be determined
2. A pressure gauge located at the bottom of the chamber above the test valve to confirm liquid recovery in the chamber.

III. Design Factors and Simulated Tests

Strictly speaking, the aims of CCDST do not differ from those of DST, and the same information can be gained from both procedures. The CCDST simply provides a more rigorous basis for rate determination, particularly for gas wells, along with the previously stated advantages of safety and security.

An attractive feature of CCDST is that the test may be switched to conventional DST i.e., the surface valve may be opened at any point during flow periods. A common procedure is to start a test as closed-chamber and then switch to open surface flow during the second or subsequent flow periods. The prior DST discussion concerning length of flow and shut-in applies to CCDST. However, often a short first flow period of 10-15 minutes is used. Alexander[26] presents a detailed pre-CCDST design for maximum fluid influx and corresponding expected surface pressure rise.

Fig. 27 is a CCDST well configuration schematic.

Figs. 28-31 present downhole and surface pressure responses for several theoretical closed-chamber responses. The simulations do not consider chamber blowdown during the buildup portions of the test. The first two figures (28 and 29) are responses for 100% liquid production. The two cases differ only by permeability. Notice the very minor rise in surface pressure, which confirms no free gas production. Figs. 30 and 31 represent 100% gas production for a high and medium permeability case, respectively. For the high permeability case (Fig. 30) the surface and bottomhole pressure increased rapidly and, in fact, returned to static conditions prior to the closed-in period. The medium permeability case (Fig. 31) does not have as sharp a pressure rise.

IV. Analysis Methods and Sample Test

Semilog and type curve methods are applicable to CCDST pressure buildup analysis. The surface pressure response during the flow periods (surface valve closed) provides an excellent indication of the fluid influx at the sandface. Alexander[26] provides a methodology to determine if the surface pressure response is consistent with 100% gas production, 100% gas-free water production, or something in between such as gassy water or liquid hydrocarbons. The surface pressure behavior is predicted through real gas laws and knowledge of the chamber volume. Rates may be determined by using the change in surface pressure with time (dp/dt) and liquid influx. Charts and equations[26] are presented for determining rate during CCDST flow periods.

The closed-chamber test example below was performed on a coalbed methane well. Rock, fluid data, and pertinent test data are shown in Table 11. Final buildup period processed data are presented in Table 12. To analyze the data the following steps are taken:

1. The downhole gauge pressure/time plot (Fig. 32) strongly suggests the initial closed-in period does not have the "closure" necessary for analysis and appears to be storage-dominated. Therefore we will not attempt analysis on this period.

2. In order to plot the second buildup using equivalent time, the rates during the test must be calculated from the surface pressure response. Fig. 33 is a plot of surface pressure during the test. Alexander[26] gave the following equation for 100% pure gas influx cases when the surface valve is closed and the test valve is open:

$$q = (\frac{286}{Tz})(V_{ch}\frac{dp}{dt}) \tag{22}$$

The average dp/dt during the first flow is 0.066 psia/min while for the second flow dp/dt is 0.064 psia/min

$$\therefore,\ q_1 = \frac{(286)(54.22)(0.066)}{(76+460)(0.95)} = 2.01\ Mscf/D$$

and

$$q_2 = \frac{(286)(54.22)(0.064)}{(76+460)(0.95)} = 1.95\ Mscf/D$$

3. A derivative log-log plot of the second buildup utilizing pseudopressure and equivalent pseudotime is shown in Fig. 34. At this point the analysis may be ended because the derivative log-log plot suggests that storage effects probably corrupted the equivalent time function.[18] A semilog plot for the second buildup period is shown in Fig. 35.

Also, the test cannot be analyzed by the techniques presented in this paper due the fact that during 100% gas flow, the pressure/rate/time relationship is not adequately described by the diffusivity equation. Therefore any test interpretation is questionable.[27]

SURGE TEST

I. Description and Purpose

The surge test is a limiting form of the previously described closed-chamber flow period. Originally conducted in offshore Gulf Coast wells, backsurge perforation washing and underbalanced perforating served to clean up the well, enabling higher productivity well completions. Recent advances[28-33] in analysis techniques allow the surge pressure data to be analyzed.

Surge tests are typically shorter than DSTs but allow for a rapid initial assessment of a zone with a relatively small amount of production. The tests can provide good estimates for permeability and even better estimates of initial pressure. A fluid sample may be retrieved, also. A pressure/time trace of a typical surge is shown in Fig. 36.

II. Basic Tools and Instrumentation

Petak, et al.[28], Simmons[30], and Mfonfu and Grader[31] provide schematic diagrams of typical surge test tool configurations and instrumentation which include:

1. **Valves** - The formation surges against the upper valve when the lower valve is opened.
2. **Packer** - isolates zone of interest.
3. **Pressure gauge** - run in the chamber and/or blanked-off below the lower valve. Usually is of the electronic variety due to the rapid pressure changes which require accurate measurements.
4. **Chamber** - entraps the surged fluid volume and is comprised of the available gas or air-filled drillstring below the upper valve.

The chamber may contain an initial liquid cushion in addition to the air or nitrogen cushion. As liquid enters the chamber the available gas cushion is compressed and formation flow decreases as pressure builds back to static reservoir pressure within the chamber.

Surges are normally conducted on cased wells. A surge test well configuration is presented in Fig. 37.

III. Design Factors and Simulated Tests

The surge test is a backpressure test with constantly changing rates. This would appear to present problems from an analysis standpoint due to the need for determining a declining rate schedule for superposition. Fortunately, the analysis method used below relies on total volume produced during the surge and not on rate determination. Therefore, no problem exists as far as determining the length of flow and closed-in periods for design purposes. However, the chamber should be properly sized to assure true surge behavior, i.e., the reservoir fluid produced into the chamber compresses the available gas cushion and sandface flow decreases to practically zero.

Soliman's method[32,33] of surge analysis assumes that the production time is very small compared to the total test duration, and that the chamber completely fills with reservoir fluid. Therefore, it would appear that small chamber volume tests are more effective since such chambers would fill faster, thus shortening overall test time. However, a distinct advantage exists when operators employ larger chamber volumes. With larger chamber volumes (implying more produced volume during the test) the producing formation has a better chance of cleaning up the non-indigenous fluids which cause skin damage while sampling a larger volume of reservoir.

The following recommendations based on experience should provide some general guidelines when considering a surge test.

1. The analysis[32,33] described below depends on the late time data of the surge period. The chamber should be properly sized to assure meaningful results in a reasonable amount of time. Therefore the use of a surge test design package (simulator) to evaluate various scenarios is recommended.
2. Highly sensitive electronic pressure recorders are usually necessary to measure the response, particularly the small pressure changes at late times.
3. Although not precluded by theory, gas zones do not appear to produce results as amenable to analysis as oil zones.
4. The best applications appear to be in relatively highly permeable liquid wells as per the earlier description of the use in Gulf Coast wells.
5. Multiple surges allow for cross checking of results.

Figs. 38 and 39 illustrate theoretical pressure responses for liquid well surge tests. The different responses shown in Fig. 38 are due to different permeabilities. Notice that for the lower permeability case, the response is essentially a slug flow until the air cushion is compressed. At that point, pressure begins building more rapidly. Fig. 39 shows a single permeability case for three values of skin. Chamber fillup will be slower for lower productivity cases; e.g. for either low permeability or high skin damage.

IV. Analysis Methods and Sample Test

Soliman's method is analytical, graphical, and allows for rapid analysis of short producing time tests provided that the total test time ($t_p+\Delta t$) is much greater than the production time, t_p. The late time pressure data are used for extrapolation and permeability calculation. This method involves making a series of three plots to identify flow regime, to obtain extrapolated pressure, and finally to calculate permeability. Skin cannot be calculated.

The surge test field data below represent a good example of radial flow response. A pressure/time graph (Fig. 40) shows the test response. Rock and fluid data are presented in Table 13 and results in Table 14. (Due to the large number of data points used in the analysis, the data are not presented in this paper.) To perform the analysis the following steps are taken:

1. The derivative log-log plot (Fig. 41) indicates a negative unit slope at late time, confirming radial flow.
2. The Cartesian plot (Fig. 42) is constructed,utilizing the radial flow time function, $1/\Delta t$. An expanded plot (Fig. 43) reveals a linear portion of late time data which extrapolates to 2774.4 psia (infinite shut-in time ($1/\infty=0$) on the abscissa).
3. To calculate permeability a log-log plot of (p_i-p_{wf}) vs Δt is constructed (Fig. 44). For radial flow, the late time data should have a negative unit slope on the log-log plot. From the negative unit slope line drawn on the plot, a value of Δp at Δt of one hour is determined to be 5.05 psia. The following equation is used to calculate permeability for radial flow cases.

$$k = \frac{1694.4\ V_{ch}\mu}{h(p_i-p_{wf})_{\Delta t=1hr}} \tag{23}$$

$$k = \frac{1694.4(1.77)(0.427)}{26(5.05)} = 9.8\ md$$

SLUG TEST

I. Description and Purpose

The slug test was introduced by Ferris and Knowles[34] in the field of groundwater hydrology in 1954, and this test is performed by allowing a reservoir to produce liquid into tubing or drill collars/drillpipe while open at the surface. Once liquid flows at the surface, slug flow no longer exists and true pressure drawdown commences. The only technical difference between slug and surge tests is that surge tests employ a closed surface valve or closed chamber. Both tests are backpressure tests but due to the closed chamber and air compression, surge tests build back to static reservoir pressure faster than slug tests. Fig. 13 includes the slug flow portion of a typical DST.

Realistically speaking, slug tests are not as useful as the three previously described tests, and probably occur as often by accident as by direct planning. Fluid samples, permeability, skin, and initial pressure are theoretically available on slug tests; however certain analysis techniques may preclude determination of initial pressure or skin.

II. Basic Tools and Instrumentation

The slug test requires essentially the same tools and instrumentation that the DST employs.

III. Design Factors and Simulated Tests

From a design standpoint the slug test appears easier to manage since there is no concern for length of time for a following buildup. Surface "blow" should provide an indication of the rate of liquid influx into the drillpipe. Obviously, pressure will increase faster for fillup of smaller ID pipe and for higher gradient fluid. In the DST section, it was seen that liquid wells exhibit slug flow during the flow periods and this slug flow may be analyzed as a slug test. When reservoir pressure, will not support a full column of liquid however; the hydrostatic backpressure will "equalize" with reservoir pressure, killing the well.

Fig. 45 shows a slug flow period with a gentle curvature that is indicative of subcritical flow. As liquid head increases inside the drillpipe, backpressure on the formation increases and the rate of liquid influx decreases. The diffusivity equation dictates that an increase in bottomhole flowing pressure must be accompanied by a decrease in flow rate. Fig. 46 presents an actual slug flow period with a break in the rate of pressure buildup. This break results from the fluid going from small ID drill collars to larger ID drillpipe. In this case the rate of fluid influx is constant (even though backpressure increases) and the flow is called critical flow.[1,4] During critical flow the flow rate does not depend on pressure drop as such the diffusivity equation is not governing the response. Restrictive tool IDs result in critical flow conditions. Such flow data cannot be analyzed; however, an ensuing buildup can be analyzed. Fig. 47 presents a high permeability slug test. This situation is similar to surge behavior.

IV. Analysis Methods and Sample Test

Ramey, et al.[35] presented a type curve method for analysis of slug test data. (For a more thorough treatment of the type-curve method applied in this example, see Earlougher[4].) Soliman[36] presented a slug analysis method which utilizes an equivalent buildup. The short producing time technique used to analyze surge data may sometimes apply to slug test data. For the case presented below, the Ramey, et al. slug flow type curve is used for evaluation. The simulator[37] was employed to generate the slug flow data represented in Fig. 48. Simulator input data are given in Table 15 while the generated pressure/time data are shown in Table 16. Results are summarized in Table 17. The type curve match is shown in Fig. 49. The following steps provide the complete analysis.

1. The recorded match parameters are

   $(C_De^{2S})_M = 10^6$, $t_M = 1.47$ hr, $(t_D/C_D)_M = 10$

2. To calculate the storage coefficient

$$C = \frac{V_\mu}{\left(\frac{\rho}{144}\frac{g}{g_c}\right)} \tag{24}$$

$$C = \frac{0.00579}{\left(\frac{62.3}{144}\frac{32.2}{32.2}\right)}$$

   C = 0.0134 bbl/psi

3. To calculate permeability

$$k = 3389 \frac{\mu}{h} \frac{C}{t_M} (\frac{t_D}{C_D}) \tag{25}$$

$$k = 3389(\frac{1}{10})(\frac{0.0134}{1.47})(10) = 30.9 \; md$$

4. To calculate skin

$$s = ½ \ln [\frac{\phi c_t h r_w^2 (C_D e^{2S})_M}{0.89359C}] \tag{26}$$

$$s = ½ \ln [\frac{0.10(8x10^{-6})(10)(.5)^2 10^6}{0.89359(0.0134)}]$$

$$s = +2.6$$

The above values agree with the simulator input.

CONCLUSIONS

The tests described in this paper provide operators of oil and gas wells valuable information. By performing pressure transient tests, an operator may determine if a well's initial poor performance is due to low permeability and/or skin damage. These parameters guide decisions concerning potential well stimulation and the design of such stimulation, or may lead to the plugging and abandonment of the well. Future field studies (reservoir simulation, material balance) make judicious use of initial pressure. Although well testing should be considered throughout the life of a well, early testing is as critical as any future testing.

Even though these short term tests are relatively less costly to run than longer tests, no less consideration should be given to the type of equipment and test time necessary for a good test. Testing companies should be able to provide operators with appropriate testing procedures, if requested, to enhance the possibilities for a good, conclusive well test.

NOMENCLATURE

B	Formation volume factor, RB/STB
C	Wellbore storage coefficient, RB/psi (Eqs. 10 & 24) Choke coefficient, Mscf/D/psia (Eq. 18)
C_D	Wellbore storage coefficient, dimensionless
c_t	Total system compressibility, psi^{-1}
c_{wb}	Wellbore fluid compressibility, psi^{-1}
g	Acceleration of gravity, ft/sec^2
g_c	Units conversion factor, 32.17 $lb_m\ ft/(lb_f sec^2)$
h	Formation thickness, ft
k	Formation permeability, md (refers to fluid permeability in analysis examples)
m	Semilog slope, psi/cycle or $MMpsi^2$/cp/cycle
$m(p)$	Gas pseudopressure, psi^2/cp
p	Pressure, psi
p_b	Base pressure, psi
p_D	Pressure, dimensionless
p_i	Initial reservoir pressure, psi
p_o	Pressure in pipe prior to DST flow period, psi
p_{wf}	Bottomhole flowing pressure, psi
p_{ws}	Bottomhole shut-in pressure, psi
p_1	Pressure at log cycle 1 on Horner plot, psi
p_{1hr}	Theoretical pressure one hour into test period (flow or shut-in), psi
p^*	Extrapolated pressure from buildup semilog line, psi
q	Flow rate of oil or gas, STB/D or Mscf/D
r	Radius, ft
r_D	Radius, dimensionless (r_e/r_w)
r_e	External boundary radius, ft
r_w	Wellbore radius, ft
s	Skin, dimensionless
T	Temperature, °R Surface in Eq. 18 Reservoir in Eq. 20 Average chamber in Eq. 22
t	Time, hours (minutes in Eq. 15)
t_a	Pseudotime, hrs-psi/cp
t_{ae}	Equivalent pseudotime, hrs-psi/cp
t_D	Time, dimensionless
t_e	Equivalent time, hours
t_o	Base time, hrs
t_p	Production time, hours
V_{ch}	Chamber volume, bbl
V_{wb}	Wellbore volume available for storage, bbl
V_μ	Pipe capacity, bbls/ft
z	Gas compressibility factor, dimensionless

Greek Symbols

γ	Fluid gravity, dimensionless
Δ	Difference
η	Hydraulic diffusivity, ft^2/hr
μ	Viscosity, cp
ϕ	Effective porosity, fraction
ρ	Density, lb/ft^3
π	3.14159...

REFERENCES

1. Matthews, C.S. and Russell, D.G.: Pressure Buildup and Flow Tests in Wells, Monograph Series, SPE, Richardson, TX (1967) 1.
2. Lee, John: Well Testing, Textbook Series, SPE, Richardson, TX (1982).
3. Horne, R.N.: Modern Well Test Analysis - A Computer Aided Approach, Petroway, Inc., Palo Alto, CA, (1990).
4. Earlougher, R.C., Jr.: Advances in Well Test Analysis, Monograph Series, SPE, Richardson, TX (1977) 5.
5. Muskat, M.: The Flow of Homogeneous Fluids Through Porous Media, McGraw-Hill Book Co., Inc., New York (1937).
6. van Everdingen, A.F. and Hurst, W.: "The Application of the Laplace Transformation to Flow Problems in Reservoirs", Trans., AIME (1949) 186, 305-324.
7. Horner, D.R.: "Pressure Build-Up in Wells", Proc., Third World Pet. Cong., E.J. Brill, Leiden (1951) II, 503.
8. Carslaw, H.S. and Jaeger, J.C.: Conduction of Heat in Solids, Oxford at the Clarendon Press (1959).
9. Theis, C.V.: "The Relation Between the Lowering of The Piezometric Surface and the Rate and Duration of Discharge of a Well Using Ground-Water Storage," Trans., AGU (1935) 519-524.
10. Ramey, H.J., Jr.: "Short-Time Well Test Data Interpretation in the Presence of Skin Effect and Wellbore Storage," JPT (Jan. 1970) 97-104.
11. Agarwal, R.G., Al-Hussainy, R., and Ramey, H.J., Jr.: "An Investigation of Wellbore Storage and Skin Effect in Unsteady Liquid Flow: I. Analytical Treatment," SPEJ (Sept. 1970) 279-290; Trans., AIME, 249.
12. Wattenbarger, R.A. and Ramey, H.J., Jr.: "An Investigation of Wellbore Storage and Skin Effect in Unsteady Liquid Flow: II. Finite Difference Treatment," SPEJ (Sept. 1970) 291-297; Trans., AIME, 249.
13. van Everdingen, A.F.: "The Skin Effect and Its Influence on the Productive Capacity of a Well," Trans., AIME (1953) 198, 171-176.
14. Hurst, W.: "Establishment of the Skin Effect and Its Impediment to Fluid Flow Into a WellBore," Pet. Eng. (Oct. 1953) B-6 through B-16.
15. Hawkins, M.F., Jr.: "A Note on the Skin Effect," Trans., AIME (1956) 207, 356-357.
16. Gringarten, A.C., Bourdet, D., Landel, P.A., and Kniazeff, V.: "A Comparison Between Different Skin and Wellbore Storage Type Curves for Early-Time Transient Analysis," paper SPE 8205 presented at the 1979 SPE Annual Technical Conference and Exhibition, Las Vegas, NV, Sept. 23-26.
17. Bourdet, D., Ayoub, J.A., and Pirard, Y.M.: "Use of the Pressure Derivative in Well Test Interpretation," SPE Formation Evaluation (June 1989) 293-302.
18. Agarwal, R.G.: "A New Method to Account for Producing Time Effects When Drawdown Type Curves are Used to Analyze Pressure Buildup and Other Test Data," paper SPE 9289 presented at the 1980 SPE Annual Technical Conference and Exhibition, Dallas, TX, Sept. 21-24.
19. Al-Hussainy, R. and Ramey, H.J., Jr.: "Application of Real Gas Flow Theory to Well Testing and Deliverability Forecasting," JPT (May 1966) 637-642, Trans., AIME (237).
20. Agarwal, R.G.: "Real Gas Pseudotime - A New Function for Pressure Buildup Analysis of Gas Wells," paper SPE 8279 presented at the 1979 SPE Annual Technical Conference and Exhibition, Las Vegas, NV, Sept. 23-26.
21. Muskat, M.: "Use of Data on the Build-Up of Bottomhole Pressures," Trans., AIME (1937) 123, 44-48.
22. Miller, C.C., Dyes, A.B., and Hutchinson, C.A., Jr.: "The Estimation of Permeability and Reservoir Pressure From Bottom-Hole Pressure Build-Up Characteristics," Trans., AIME (1950) 189, 91-104.
23. Koederitz, L.F.: Notes on Well Test Analysis, University of Missouri-Rolla, (July 1985).
24. Murphy, W.C.: "The Interpretation and Calculation of Formation Characteristics from Formation Test Data," Pamphlet T-101, Halliburton Services, Duncan, OK. (1970).
25. Fulton, D.D.: "A Primer of DST Chart Interpretation," Halliburton Reservoir Services Technical Presentation HRS 4086.

26. Alexander, L.G.: "Theory and Practice of the Closed-Chamber Drillstem Test Method," JPT (Dec. 1977) 1539-1544.
27. Kamal, M.M. and Six, J.L.: "Pressure Transient Testing of Methane Producing Coalbeds," paper SPE 19789 presented at the 1989 SPE Annual Technical Conference and Exhibition, San Antonio, TX, Oct. 8-11.
28. Petak, K.R., Prasad, R.K., and Coble, L.E.: "Surge Test Simulation," paper SPE 21832 presented at the Rocky Mountain Regional Meeting and Low-Permeability Reservoirs Symposium held in Denver, CO, Apr. 15-17, 1991.
29. Simmons, J.F., and Sageev, A.: "Application of Closed Chamber Theory to Backsurge Completion Testing," SPE Production Engineering (Nov. 1988) 527-535.
30. Simmons, J.F.: "Interpretation of Underbalanced Surge Pressure Data by Rate-Time Convolution," JPT (Jan. 1990) 74-83.
31. Mfonfu, G.B.S., and Grader, A.S.: "An Implicit Numerical Model for the Closed Chamber Test," SPE 19832 presented at the 1989 SPE Annual Technical Conference and Exhibition, San Antonio, TX, Oct. 8-11.
32. Soliman, M.Y.: "Analysis of Buildup Tests With Short Producing Time," SPE Formation Evaluation (Aug. 1986) 363-371.
33. Soliman, M.Y., and Petak, K.R.: "Method Analyzes Pressure for Short Flow Times," Oil and Gas Journal (Apr. 30, 1990) 49-54.
34. Ferris, J.G., and Knowles, D.B.: "The Slug Test for Estimating Transmissibility," USGS Ground Water Note 26, 1-7, 1954.
35. Ramey, J.J., Jr., Agarwal, R.G., and Martin, I.: "Analysis of 'Slug Test' or DST Flow Period Data," J.C. Pet. Tech. (July-Sept., 1975) 37-47.
36. Soliman, M.Y.: "New Technique for Analysis of Variable Rate or Slug Test," paper SPE 10083 presented at the 1981 SPE Annual Technical Conference and Exhibition, San Antonio, TX, Oct. 5-7.
37. Halliburton Reservoir Services Well Test Simulator "RTZ"

ACKNOWLEDGEMENTS

We express our appreciation to the managements of Halliburton Reservoir Services and Halliburton Services for permission to publish this paper. We also commend David Parnell and Rayleene Morris for their assistance in the production of the paper. Thanks to all others who offered suggestions and support.

Table 1
Oil DST Field Case: Basic Reservoir Properties and Test Information

Effective Porosity	10%	Pay Thickness, ft	12
Reservoir Temperature, °F	131	Wellbore Radius, ft	0.345
Oil Formation Volume Factor, RB/STB	1.545	System Compressibility, $MMpsi^{-1}$	22.91
Oil Viscosity, cp	0.33	Pipe Capacity, bbls/ft	0.00492
Oil Density, lb/ft^3	48.8		

Table 2
Oil DST Field Case: Time and Pressure

t, hrs	p, psig
0.000	46.5
0.050	40.7
0.100	40.7
0.150	43.6
0.200	46.6
0.250	48.9
0.300	51.0
0.350	53.5
0.400	53.5
0.450	57.6
0.505	61.8
0.522	141.7
0.538	200.5
0.555	259.5
0.572	318.1
0.588	365.0
0.605	440.7
0.622	503.6
0.638	569.4
0.655	639.9
0.672	706.1
0.705	853.5
0.738	1009.4
0.772	1134.9
0.805	1287.7
0.855	1477.6
0.905	1666.4
0.938	1778.9
0.972	1882.2
1.005	1977.4
1.088	2160.5
1.172	2297.2
1.257	2391.7
1.338	2447.5
1.422	2482.8
1.487	2499.6
1.487	63.2
1.537	64.3
1.587	79.4
1.637	83.6
1.687	85.7
1.737	87.9
1.787	91.0
1.837	93.7
1.887	96.3
1.937	99.3
1.987	101.3
2.037	105.5
2.087	108.1
2.137	110.5
2.187	111.6
2.237	115.8
2.287	118.5
2.337	122.0
2.387	123.5
2.437	126.8
2.505	128.6
2.522	349.7
2.538	490.2
2.555	619.3
2.572	766.7
2.588	931.4
2.605	1111.6
2.622	1267.2
2.638	1449.7
2.655	1580.5
2.672	1711.0
2.705	1922.0
2.738	2096.0
2.772	2217.0
2.805	2307.1
2.838	2364.2
2.872	2398.6
2.905	2422.0
2.938	2441.6
2.972	2452.2
3.005	2459.6
3.088	2473.8
3.172	2484.5
3.255	2488.5
3.338	2493.5
3.422	2497.0
3.505	2498.8
3.672	2505.3
3.838	2509.9
4.005	2511.5
4.172	2515.6
4.338	2516.3
4.500	2517.8

Table 3
Oil DST Field Case: Buildup No. 1, Processed Data

Δt, hrs	p_{ws}, psig	Δt_e, hrs	Δp, psi	$\frac{t+\Delta t}{\Delta t}$
0.000	61.8	*	0.0	*
0.017	141.7	0.968	79.9	31.300
0.033	200.5	1.876	138.7	16.150
0.050	259.5	2.730	197.7	11.100
0.067	318.1	3.534	256.3	8.575
0.083	365.0	4.292	303.2	7.060
0.100	440.7	5.008	378.9	6.050
0.117	503.6	5.686	441.8	5.329
0.133	569.4	6.328	507.6	4.788
0.150	639.9	6.938	578.1	4.367
0.167	706.1	7.519	644.3	4.030
0.200	853.5	8.596	791.7	3.525
0.233	1009.4	9.577	947.6	3.164
0.267	1134.9	10.470	1073.1	2.894
0.300	1287.7	11.293	1225.9	2.683
0.350	1477.6	12.403	1415.8	2.443
0.400	1666.4	13.389	1604.6	2.263
0.433	1778.9	13.995	1717.1	2.165
0.467	1882.2	14.553	1820.4	2.082
0.500	1977.4	15.075	1915.6	2.010
0.583	2160.5	16.238	2098.7	1.866
0.667	2297.2	17.236	2235.4	1.758
0.752	2391.7	18.122	2329.9	1.672
0.833	2447.5	18.867	2385.7	1.606
0.917	2482.8	19.536	2421.0	1.551
0.982	2499.6	20.013	2437.8	1.514

Producing Time = 0.505 hr

Table 4
Oil DST Field Case: Buildup No. 2, Processed Data

Δt, hrs	p_{ws}, psig	Δt_e, hrs	Δp, psi	$\frac{t+\Delta t}{\Delta t}$
0.000	128.6	*	0.0	*
0.017	349.7	0.989	221.1	92.400
0.033	490.2	1.957	361.6	46.700
0.050	619.3	2.905	490.7	31.467
0.067	766.7	3.832	638.1	23.850
0.083	931.4	4.741	802.8	19.280
0.100	1111.6	5.631	983.0	16.233
0.117	1267.2	6.502	1138.6	14.057
0.133	1449.7	7.356	1321.1	12.425
0.150	1580.5	8.193	1451.9	11.156
0.167	1711.0	9.014	1582.4	10.140
0.200	1922.0	10.607	1793.4	8.617
0.233	2096.0	12.140	1967.4	7.529
0.267	2217.0	13.615	2088.4	6.713
0.300	2307.1	15.038	2178.5	6.078
0.333	2364.2	16.409	2235.6	5.570
0.367	2398.6	17.730	2270.0	5.155
0.400	2422.0	19.010	2293.4	4.808
0.433	2441.6	20.244	2313.0	4.515
0.467	2452.2	21.435	2323.6	4.264
0.500	2459.6	22.585	2331.0	4.047
0.583	2473.8	25.312	2345.2	3.611
0.667	2484.5	27.823	2355.9	3.285
0.750	2488.5	30.155	2359.9	3.031
0.833	2493.5	32.320	2364.9	2.828
0.917	2497.0	34.335	2368.4	2.662
1.000	2498.8	36.227	2370.2	2.523
1.167	2505.3	39.636	2376.7	2.306
1.333	2509.9	42.651	2381.3	2.143
1.500	2511.5	45.337	2382.9	2.016
1.667	2515.6	47.753	2387.0	1.914
1.833	2516.3	49.918	2387.7	1.831
1.995	2517.8	51.814	2389.2	1.764

Producing Time = 1.523 hr

Table 5
Oil DST Field Case: Analysis Results

p^*, psig	2546.9
Oil Permeability, md	1.13
Skin, dim.	+19.6

Table 6
Gas DST Field Case: Basic Reservoir Properties and Test Information

Effective Porosity,	10%	Pay Thickness, ft	10
Reservoir Temperature, °F	180	Wellbore Radius, ft	0.365
Surface Temperature, °F	80	System Compressibility, $MMpsi^{-1}$	148.9
Gas Gravity, dim	0.6	Choke Coefficient*(0.25"), Mscf/D/psia	26.51
Gas Viscosity, cp	0.021		

**6" Positive Choke*

Table 7
Gas DST Field Case: Time and Pressure

t, hrs	p, psig	t, hrs	p, psig
0.000	39.7	1.793	1018.5
0.050	40.0	1.810	1482.3
0.100	40.0	1.827	1863.7
0.150	40.0	1.843	2166.9
0.200	40.0	1.860	2407.9
0.257	39.7	1.877	2597.5
0.273	177.0	1.893	2730.4
0.290	365.2	1.910	2858.5
0.307	651.0	1.927	2991.4
0.323	1006.7	1.960	3235.1
0.340	1301.4	1.993	3406.5
0.357	1509.8	2.027	3555.4
0.373	1777.0	2.060	3659.0
0.390	1973.2	2.093	3745.7
0.407	2190.0	2.127	3817.2
0.423	2350.8	2.160	3862.7
0.457	2604.3	2.193	3902.8
0.490	2803.5	2.227	3935.0
0.523	2993.5	2.260	3960.8
0.557	3152.1	2.343	4000.1
0.590	3288.6	2.427	4022.7
0.623	3408.2	2.510	4036.4
0.657	3516.0	2.593	4045.2
0.690	3607.1	2.677	4051.7
0.712	3645.5	2.760	4055.5
0.712	24.1	2.927	4060.9
0.795	24.8	3.093	4064.5
0.878	36.4	3.260	4066.5
0.962	43.3	3.427	4068.0
1.045	48.5	3.467	4068.2
1.128	52.1		
1.212	55.3		
1.295	55.3		
1.378	55.3		
1.462	56.9		
1.545	56.9		
1.628	56.9		
1.712	59.4		
1.760	58.2		
1.777	496.1		

Table 8
Gas DST Field Case: Buildup No. 1, Processed Data

Δt, hrs	m(p), $MMpsia^2/cp$	Δt_e, hrs	$\Delta m(p)$, $MMpsia^2/cp$	$\frac{t+\Delta t}{\Delta t}$
0.000	0.2052	*	0.0000	*
0.017	2.7466	0.939	2.5413	16.400
0.033	10.8719	1.770	10.6667	8.700
0.050	33.4681	2.511	33.2629	6.133
0.067	78.5519	3.175	78.3467	4.850
0.083	129.5410	3.775	129.3360	4.080
0.100	172.6040	4.317	172.3990	3.567
0.117	235.6780	4.813	235.4730	3.200
0.133	287.1680	5.265	286.9630	2.925
0.150	348.6800	5.681	348.4750	2.711
0.167	397.1530	6.063	396.9470	2.540
0.200	477.9620	6.746	477.7570	2.283
0.233	544.8020	7.333	544.5970	2.100
0.267	610.9450	7.845	610.7400	1.963
0.300	667.7340	8.297	667.5291	1.856
0.333	717.6360	8.701	717.4310	1.770
0.367	762.0640	9.059	761.8590	1.700
0.400	802.6240	9.379	802.4180	1.642
0.433	837.2510	9.673	837.0450	1.592
0.455	851.9370	9.847	851.7320	1.564

Producing Time = 0.257 hr

Table 9
Gas DST Field Case: Buildup No. 2, Processed Data

Δt, hrs	$m(p)$, $MMpsia^2/cp$	Δt_e, hrs	$\Delta m(p)$, $MMpsia^2/cp$	$\frac{t + \Delta t}{\Delta t}$
0.000	0.3818	*	0.0000	*
0.017	19.6917	0.987	19.3100	79.300
0.033	80.3614	1.950	79.9796	40.150
0.050	166.6040	2.889	166.2220	27.100
0.067	257.9170	3.806	257.5350	20.575
0.083	341.9100	4.700	341.5280	16.660
0.100	414.9050	5.573	414.5230	14.050
0.117	475.7290	6.425	475.3480	12.186
0.133	519.9590	7.258	519.5770	10.788
0.150	563.7220	8.072	563.3410	9.700
0.167	610.2020	8.868	609.8200	8.830
0.200	697.9710	10.405	697.5890	7.525
0.233	761.4280	11.876	761.0460	6.593
0.267	817.5620	13.285	817.1801	5.894
0.300	857.1120	14.636	856.7310	5.350
0.333	890.4970	15.931	890.1150	4.915
0.367	918.2110	17.175	917.8290	4.559
0.400	935.9280	18.367	935.5460	4.263
0.433	951.5930	19.517	951.2110	4.012
0.467	964.2050	20.627	963.8230	3.796
0.500	974.3310	21.690	973.9490	3.610
0.583	989.7890	24.189	989.4070	3.237
0.667	998.6970	26.471	998.3150	2.958
0.750	1004.1000	28.577	1003.7200	2.740
0.833	1007.5800	30.514	1007.2000	2.566
0.917	1010.1500	32.302	1009.7600	2.424
1.000	1011.6500	33.970	1011.2700	2.305
1.167	1013.7800	36.951	1013.4000	2.119
1.333	1015.2100	39.565	1014.8199	1.979
1.500	1016.0000	41.872	1015.6200	1.870
1.667	1016.5900	43.915	1016.2100	1.783
1.707	1016.6700	44.363	1016.2900	1.765

Producing Time = 1.305 hr

Table 10
Gas DST Field Case: Analysis Results

$m(p^*)$, MMpsia	1037.5
p^*, psia	4135
Gas Permeability, md	0.086
Skin, dim.	+13.2

Table 11
CCDST Field Case: Basic Reservoir Properties and Test Information

Reservoir Temperature, °F	126	Pay Thickness, ft	33
Effective Porosity,	≈5%	Wellbore Radius, ft	0.354
Gas Gravity, dim.	0.65	System Compressibility, $MMpsi^{-1}$	≈524
Z Factor, dim.	0.95	Chamber Volume, Bbls	54.22
Gas Viscosity, cp	0.016	Average Chamber Temperature, °F	76
First Flow Period Surface Pressure Change with Time, psia/min	0.066	Second Flow Period Surface Pressure Change with Time, psia/min	0.064

Table 12
CCDST Field Case: Processed Data

Δt, hrs	p_{wf}, psia	Δt_{as}, hrs-psia/cp	Superposition Function	m(p), MMpsia²/cp	Δm(p), MMpsia²/cp
0.000	27.17	*	*	47298	*
0.008	27.62	20.90	8.0001	49352	2054
0.025	28.49	62.33	7.0784	53420	6122
0.041	29.37	105.40	6.6353	57663	10365
0.058	30.24	148.86	6.3441	61985	14687
0.075	31.12	193.55	6.1226	66486	19188
0.091	31.97	237.70	5.9493	70955	23657
0.108	32.82	282.70	5.8030	75546	28248
0.124	33.69	329.04	5.6750	80369	33072
0.141	34.56	375.64	5.5633	85320	38022
0.158	35.42	422.24	5.4646	90337	43040
0.174	36.28	469.67	5.3748	95479	48182
0.191	37.14	517.76	5.2926	100744	53446
0.208	38.01	566.94	5.2161	106197	58899
0.224	38.86	615.57	5.1466	111646	64348
0.241	39.71	664.69	5.0819	117217	69919
0.257	40.57	714.91	5.0204	122975	75677
0.274	41.42	765.33	4.9629	128789	81491
0.291	42.27	816.27	4.9086	134723	87426
0.307	43.11	867.52	4.8572	140707	93410
0.324	43.93	919.27	4.8083	146663	99365
0.340	44.73	969.84	4.7632	152582	105284
0.357	45.61	1024.36	4.7170	159216	111918
0.373	46.44	1075.63	4.6758	165593	118295
0.390	47.30	1129.83	4.6344	172321	125023
0.407	48.13	1183.24	4.5954	178933	131635
0.423	48.95	1237.07	4.5579	185577	138280
0.440	49.78	1291.81	4.5214	192419	145121
0.456	50.59	1345.72	4.4869	199207	151909
0.473	51.40	1400.58	4.4532	206105	158808
0.490	52.21	1455.96	4.4205	213113	165815
0.515	53.44	1539.84	4.3732	223966	176668
0.531	54.25	1595.27	4.3434	231252	183954
0.548	55.06	1651.54	4.3141	238646	191348
0.564	55.86	1708.08	4.2857	246059	198761
0.581	56.66	1765.04	4.2581	253579	206281
0.598	57.45	1821.77	4.2314	261111	213813
0.614	58.23	1878.65	4.2055	268650	221353
0.631	59.01	1936.39	4.1799	276292	228994
0.648	59.79	1993.93	4.1552	284036	236738
0.664	60.57	2051.66	4.1311	291881	244583
0.681	61.34	2109.43	4.1077	299727	252430
0.706	62.49	2197.21	4.0733	311632	264334
0.722	63.26	2256.26	4.0510	319727	272429
0.739	64.01	2314.10	4.0296	327708	280410
0.755	64.77	2373.11	4.0084	335891	288593
0.772	65.53	2432.37	3.9876	344172	296874
0.789	66.29	2492.33	3.9670	352550	305252
0.805	67.02	2550.54	3.9475	360690	313392
0.830	68.14	2640.11	3.9184	373351	326053
0.847	68.89	2700.53	3.8993	381948	334650
0.863	69.62	2760.09	3.8809	390406	343108
0.880	70.34	2819.40	3.8630	398835	351537
0.896	71.07	2880.12	3.8450	407472	360174
0.913	71.78	2939.87	3.8277	415959	368661
0.938	72.86	3030.73	3.8020	429029	381731
0.954	73.58	3091.25	3.7854	437852	390554
0.971	74.29	3151.48	3.7691	446639	399341
0.988	75.00	3212.43	3.7529	455509	408212
1.004	75.71	3273.13	3.7371	464465	417167

Table 12
CCDST Field Case: Processed Data

Δt, hrs	p_{wf}, psia	Δt_{as}, hrs-psia/cp	Superposition Function	m(p), MMpsia²/cp	Δm(p), MMpsia²/cp
1.021	76.42	3333.24	3.7218	473505	426207
1.046	77.53	3424.97	3.6989	487811	440513
1.063	78.29	3486.94	3.6837	497724	450427
1.079	79.04	3547.73	3.6692	507603	460305
1.096	79.79	3609.45	3.6546	517576	470279
1.129	81.27	3732.68	3.6263	537536	490238
1.146	82.00	3793.61	3.6126	547517	500219
1.170	83.11	3887.59	3.5920	562865	515567
1.187	83.84	3949.19	3.5787	573072	525775
1.204	84.58	4011.82	3.5655	583513	536216
1.220	85.32	4073.46	3.5526	594045	546747
1.237	86.07	4136.21	3.5397	604812	557515
1.253	86.80	4197.98	3.5272	615384	568086
1.270	87.53	4260.88	3.5147	626045	578748
1.295	88.62	4354.94	3.4962	642132	594834
1.311	89.33	4416.29	3.4844	652720	605422
1.328	90.06	4479.63	3.4724	663693	616395
1.345	90.78	4542.63	3.4606	674603	627306
1.361	91.49	4605.12	3.4491	685448	638150
1.386	92.56	4700.18	3.4319	701954	654656
1.403	93.26	4762.54	3.4208	712855	665557
1.419	93.97	4826.39	3.4095	723997	676699
1.436	94.67	4889.09	3.3986	735067	687769
1.453	95.37	4952.31	3.3878	746217	698920
1.478	96.40	5045.69	3.3721	762777	715479
1.494	97.09	5109.14	3.3615	773969	726671
1.511	97.78	5172.46	3.3511	785241	737943
1.527	98.46	5235.22	3.3410	796431	749133
1.552	99.48	5331.91	3.3255	813358	766060
1.561	99.81	5362.70	3.3207	818875	771577
1.569	100.16	5395.69	3.3155	824743	777445
1.577	100.49	5426.32	3.3107	830295	782997
1.586	100.84	5457.29	3.3059	836203	788905
1.594	101.23	5489.82	3.3009	842812	795514
1.602	101.61	5521.15	3.2961	849276	801978
1.610	101.98	5552.49	3.2913	855593	808295
1.619	102.36	5584.63	3.2864	862105	814807
1.627	102.74	5616.74	3.2816	868641	821343
1.635	103.11	5648.37	3.2769	875029	827731
1.644	103.48	5680.02	3.2722	881442	834144
1.652	103.86	5712.50	3.2673	888050	840752
1.660	104.23	5743.74	3.2627	894508	847210
1.668	104.60	5775.28	3.2581	900988	853691
1.677	104.97	5807.28	3.2535	907492	860194
1.685	105.33	5838.74	3.2489	913842	866545
1.693	105.70	5871.02	3.2443	920392	873094
1.702	106.07	5903.31	3.2396	926964	879667
1.710	106.43	5934.76	3.2352	933381	886084
1.718	106.80	5967.41	3.2305	940000	892702
1.727	107.16	5998.92	3.2261	946461	899163
1.735	107.53	6030.88	3.2216	953125	905827
1.743	107.90	6062.49	3.2172	959812	912514
1.751	108.27	6094.18	3.2128	966522	919224
1.760	108.64	6126.39	3.2083	973255	925957
1.768	109.01	6157.95	3.2040	980014	932716
1.776	109.40	6191.16	3.1995	987158	939861
1.785	109.77	6222.80	3.1952	993965	946667
1.793	110.14	6254.47	3.1909	1000790	953494
1.801	110.53	6287.41	3.1865	1008010	960716

Table 12
CCDST Field Case: Processed Data

Δt, hrs	p_{wf}, psia	Δt_{ae}, hrs-psia/cp	Superposition Function	m(p), MMpsia²/cp	Δm(p), MMpsia²/cp
1.809	110.90	6318.05	3.1824	1014890	967590
1.818	111.29	6351.53	3.1779	1022160	974862
1.826	111.65	6382.02	3.1739	1028890	981596
1.834	112.04	6415.77	3.1694	1036210	988917
1.843	112.41	6447.14	3.1653	1043180	995886
1.851	112.79	6480.11	3.1610	1050370	1003070
1.859	113.16	6511.84	3.1569	1057380	1010080
1.868	113.54	6544.80	3.1526	1064610	1017310
1.876	113.91	6576.44	3.1486	1071670	1024380
1.884	114.28	6608.23	3.1445	1078760	1031460
1.909	115.40	6702.81	3.1325	1100350	1053050
1.951	117.27	6866.03	3.1122	1136870	1089570
1.976	118.37	6963.08	3.1004	1158630	1111330
2.001	119.47	7060.13	3.0887	1180600	1133300
2.017	120.21	7125.46	3.0809	1195490	1148190
2.042	121.31	7222.63	3.0695	1217790	1170500
2.067	122.41	7320.47	3.0581	1240310	1193010
2.092	123.50	7417.94	3.0470	1262820	1215520
2.108	124.22	7482.50	3.0397	1277790	1230500
2.133	125.31	7580.93	3.0287	1300640	1253340
2.158	126.38	7678.38	3.0179	1323250	1275960
2.183	127.44	7776.80	3.0071	1345860	1298560
2.200	128.14	7840.99	3.0002	1360880	1313590
2.225	129.25	7941.52	2.9894	1384880	1337590
2.249	130.35	8039.70	2.9791	1408880	1361580
2.274	131.43	8136.81	2.9690	1432630	1385330
2.291	132.16	8202.49	2.9622	1448800	1401500
2.316	133.26	8302.17	2.9520	1473330	1426030
2.341	134.32	8398.39	2.9423	1497160	1449860
2.366	135.40	8499.07	2.9322	1521640	1474340
2.383	136.10	8564.37	2.9258	1537610	1490310
2.407	137.14	8661.98	2.9162	1561500	1514200
2.432	138.20	8761.79	2.9065	1586030	1538730
2.457	139.22	8858.93	2.8972	1609810	1562520
2.482	140.24	8956.93	2.8880	1633770	1586480
2.499	140.93	9022.82	2.8818	1650080	1602790
2.524	141.98	9122.80	2.8725	1675060	1627760
2.548	143.00	9219.25	2.8636	1699500	1652200
2.573	144.05	9317.72	2.8546	1724840	1677540
2.598	145.11	9418.08	2.8456	1750610	1703310
2.615	145.79	9483.05	2.8398	1767250	1719950
2.640	146.81	9581.53	2.8311	1792340	1745050
2.665	147.85	9680.80	2.8224	1818110	1770820
2.689	148.88	9779.11	2.8139	1843820	1796520
2.714	149.90	9877.48	2.8054	1869450	1822150
2.739	150.91	9975.43	2.7971	1895010	1847710
2.756	151.58	10040.60	2.7916	1912060	1864760
2.781	152.59	10138.80	2.7834	1937900	1890600
2.806	153.60	10237.30	2.7752	1963920	1916620
2.831	154.60	10336.00	2.7672	1989850	1942550
2.856	155.58	10433.10	2.7593	2015420	1968120
2.881	156.57	10531.40	2.7514	2041420	1994120
2.897	157.23	10596.60	2.7462	2058850	2011550
2.922	158.22	10694.60	2.7384	2085130	2037830
2.947	159.20	10792.60	2.7307	2111300	2064010
2.972	160.17	10891.10	2.7230	2137380	2090080
2.997	161.12	10987.10	2.7156	2163060	2115770
3.022	162.10	11087.20	2.7080	2189720	2142430
3.046	163.05	11183.80	2.7007	2215720	2168430

Table 12
CCDST Field Case: Processed Data

Δt, hrs	p_{wf}, psia	Δt_{ae}, hrs-psia/cp	Superposition Function	m(p), MMpsia²/cp	Δm(p), MMpsia²/cp
3.071	164.00	11282.00	2.6933	2241880	2194580
3.088	164.63	11346.90	2.6884	2259310	2212010
3.113	165.58	11445.30	2.6812	2285710	2238420
3.138	166.52	11542.40	2.6740	2311990	2264700
3.163	167.46	11639.90	2.6669	2338430	2291130
3.188	168.40	11737.80	2.6599	2365010	2317710
3.213	169.33	11834.80	2.6529	2391450	2344160
3.238	170.26	11932.30	2.6460	2418050	2370750
3.262	171.18	12028.30	2.6393	2444500	2397200
3.287	172.11	12134.60	2.6318	2471390	2424090
3.296	172.39	12164.10	2.6298	2479510	2432210
3.304	172.72	12199.60	2.6273	2489100	2441800
3.312	173.02	12230.20	2.6252	2497830	2450540
3.320	173.32	12261.70	2.6230	2506590	2459290
3.329	173.64	12295.10	2.6207	2515940	2468640
3.337	173.94	12326.80	2.6186	2524720	2477420
3.345	174.24	12358.90	2.6164	2533520	2486220
3.354	174.55	12391.10	2.6142	2542620	2495320
3.362	174.87	12424.60	2.6119	2552040	2504740
3.370	175.17	12455.80	2.6098	2560890	2513590
3.379	175.48	12488.50	2.6076	2570040	2522740
3.387	175.79	12520.90	2.6054	2579210	2531920
3.395	176.09	12552.50	2.6033	2588110	2540810
3.403	176.39	12583.90	2.6012	2597010	2549710
3.412	176.70	12618.00	2.5989	2606240	2558940
3.420	176.98	12646.80	2.5970	2614570	2567280
3.428	177.31	12682.50	2.5946	2624420	2577130
3.437	177.60	12713.20	2.5925	2633090	2585800
3.445	177.89	12745.20	2.5904	2641780	2594480
3.453	178.19	12776.50	2.5884	2650780	2603480
3.461	178.51	12809.70	2.5862	2660390	2613090
3.470	178.81	12840.50	2.5841	2669430	2622130
3.478	179.11	12872.70	2.5820	2678470	2631170
3.486	179.41	12906.70	2.5798	2687530	2640230
3.495	179.67	12935.80	2.5779	2695400	2648100
3.503	179.96	12968.50	2.5758	2704190	2656890
3.511	180.27	13002.10	2.5736	2713590	2666290
3.520	180.56	13033.30	2.5716	2722410	2675110
3.528	180.85	13065.20	2.5695	2731240	2683940
3.536	181.14	13097.30	2.5674	2740080	2692780
3.544	181.42	13128.00	2.5654	2748640	2701340
3.553	181.71	13161.90	2.5633	2757510	2710210
3.561	181.97	13191.70	2.5614	2765480	2718180
3.569	182.25	13224.70	2.5593	2774070	2726770
3.578	182.53	13256.70	2.5572	2782670	2735380
3.586	182.81	13287.80	2.5552	2791300	2744000
3.594	183.11	13321.30	2.5531	2800540	2753250
3.603	183.39	13353.00	2.5511	2809190	2761900
3.611	183.65	13382.10	2.5493	2817230	2769940
3.619	183.95	13417.70	2.5470	2826530	2779230
3.628	184.20	13445.40	2.5453	2834280	2786980
3.636	184.49	13479.80	2.5431	2843290	2795990
3.644	184.77	13509.90	2.5413	2852010	2804710
3.653	185.08	13543.40	2.5392	2861670	2814370
3.661	185.38	13574.80	2.5372	2871030	2823740
3.669	185.68	13606.30	2.5353	2880420	2833120
3.677	185.98	13637.80	2.5333	2889810	2842510
3.686	186.28	13669.10	2.5314	2899220	2851920
3.694	186.58	13701.80	2.5294	2908650	2861350
3.702	186.86	13731.90	2.5275	2917460	2870160

Table 12
CCDST Field Case: Processed Data

Δt, hrs	p_{wf}, psia	Δt_{ae}, hrs-psia/cp	Superposition Function	m(p), $MMpsia^2/cp$	$\Delta m(p)$, $MMpsia^2/cp$
3.711	187.16	13764.70	2.5255	2926920	2879620
3.719	187.46	13795.50	2.5236	2936390	2889090
3.727	187.78	13829.80	2.5215	2946520	2899220
3.736	188.06	13858.70	2.5198	2955380	2908080
3.744	188.37	13891.70	2.5178	2965210	2917920
3.752	188.67	13923.00	2.5159	2974750	2927450
3.760	188.96	13953.70	2.5140	2983980	2936680
3.769	189.26	13985.80	2.5121	2993550	2946250
3.777	189.56	14018.40	2.5101	3003130	2955830
3.785	189.84	14048.40	2.5083	3012080	2964790
3.794	190.14	14081.40	2.5063	3021690	2974390
3.802	190.43	14112.60	2.5045	3031000	2983700
3.810	190.72	14144.40	2.5026	3040310	2993010
3.819	191.01	14175.80	2.5007	3049640	3002350
3.835	191.60	14240.10	2.4969	3068670	3021380
3.852	192.18	14301.90	2.4932	3087440	3040140
3.868	192.77	14366.40	2.4894	3106580	3059290
3.885	193.34	14428.80	2.4858	3125140	3077840
3.910	194.18	14521.60	2.4804	3152580	3105280
3.935	195.05	14617.30	2.4748	3181130	3133830
3.968	196.18	14743.30	2.4676	3218410	3171110
3.993	197.00	14835.20	2.4623	3245590	3198300
4.026	198.13	14963.10	2.4551	3283250	3235950
4.051	198.95	15058.60	2.4497	3310700	3263410
4.084	199.94	15175.40	2.4432	3344010	3296710
4.109	200.70	15270.80	2.4379	3369690	3322390
4.142	201.67	15391.70	2.4313	3402610	3355310
4.167	202.40	15485.80	2.4261	3427480	3380190
4.200	203.34	15607.80	2.4195	3459650	3412360
4.225	204.04	15700.60	2.4145	3483710	3436410
4.258	204.95	15819.10	2.4082	3515110	3467810
4.283	205.67	15915.00	2.4031	3540050	3492750
4.317	206.56	16030.60	2.3970	3570990	3523700
4.350	207.49	16156.80	2.3904	3603480	3556180
4.375	208.16	16247.00	2.3856	3626980	3579680
4.408	209.03	16367.30	2.3794	3657600	3610300
4.433	209.68	16457.70	2.3748	3680570	3633270
4.466	210.54	16579.10	2.3686	3711050	3663760
4.491	211.17	16668.70	2.3640	3733470	3686180
4.524	212.00	16788.50	2.3580	3763110	3715820
4.549	212.61	16877.40	2.3535	3784970	3737670
4.582	213.42	16995.50	2.3477	3814090	3766790
4.607	214.03	17085.90	2.3432	3836090	3788800
4.640	214.81	17200.70	2.3375	3864320	3817030
4.674	215.61	17320.80	2.3317	3893390	3846090
4.698	216.19	17407.40	2.3275	3914530	3867230
4.732	216.97	17526.50	2.3217	3943040	3895740
4.756	217.53	17610.40	2.3177	3963580	3916280
4.790	218.33	17734.70	2.3117	3993010	3945710
4.815	218.88	17818.10	2.3078	4013310	3966010
4.848	219.63	17935.60	2.3022	4041070	3993770
4.873	220.19	18021.60	2.2982	4061860	4014570
4.906	220.93	18136.60	2.2928	4089420	4042120
4.939	221.66	18251.00	2.2875	4116690	4069400
4.964	222.20	18334.80	2.2837	4136930	4089630
4.989	222.74	18428.20	2.2794	4157210	4109920
4.997	222.89	18456.10	2.2781	4162860	4115560

Table 13
Surge Test Field Case: Basic Reservoir Properties and Test Information

Effective Porosity,	11%	Pay Thickness, ft	26
Oil Formation Volume Factor, RB/STB	1.326	Chamber Volume, Bbls	1.77
Oil Viscosity, cp	0.427	Total Comprĕssibility, $MMpsi^{-1}$	47

Table 14
Surge Test Field Case: Analysis Results

p^*, psia	2774.4
Oil Permeability, md	9.8

Table 15
Simulated Water Zone Slug Test: Input Data

Initial Pressure, psia	2600	Pay Thickness, ft	10
Permeability, md	30	Wellbore Radius, ft	0.5
Skin, dim.	+2	Viscosity, cp	1.0
Effective Porosity	10%	System Compressibility, $MMpsi^{-1}$	8
Formation Volume Factor, RB/STB	1.05	Pipe Capacity, bbls/ft	0.00579
Water Density, lb/ft^3	62.3		

Table 16
Simulated Water Zone Slug Test: Time, Pressure, Dimensionless Pressure

t, hrs	p, psia	p_{DR}, dim.
0.0033	28.9650	0.9942
0.0270	93.0940	0.9684
0.0551	160.3230	0.9414
0.0878	232.6750	0.9123
0.1234	306.3770	0.8826
0.1724	401.4100	0.8444
0.2209	489.4270	0.8090
0.2605	557.1210	0.7817
0.3068	632.6000	0.7514
0.3613	716.2510	0.7177
0.4252	808.2880	0.6807
0.5002	908.7190	0.6403
0.6044	1036.1040	0.5890
0.7301	1173.4250	0.5338

Table 17
Simulated Water Zone Slug Test: Analysis Results

Permeability, md	30.9
Skin, dim.	+2.6

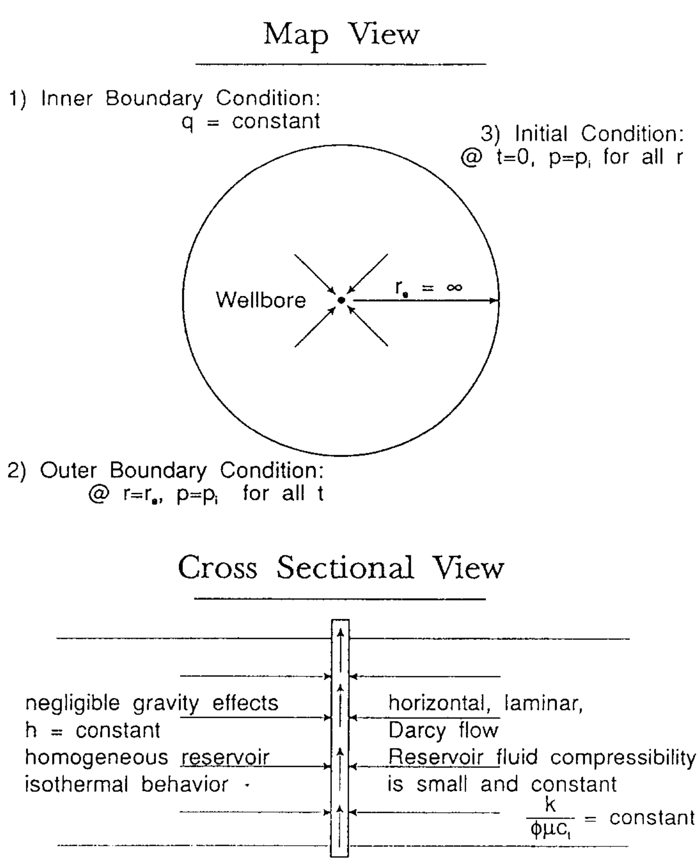

Figure 1 - Infinite-acting radial flow schematic

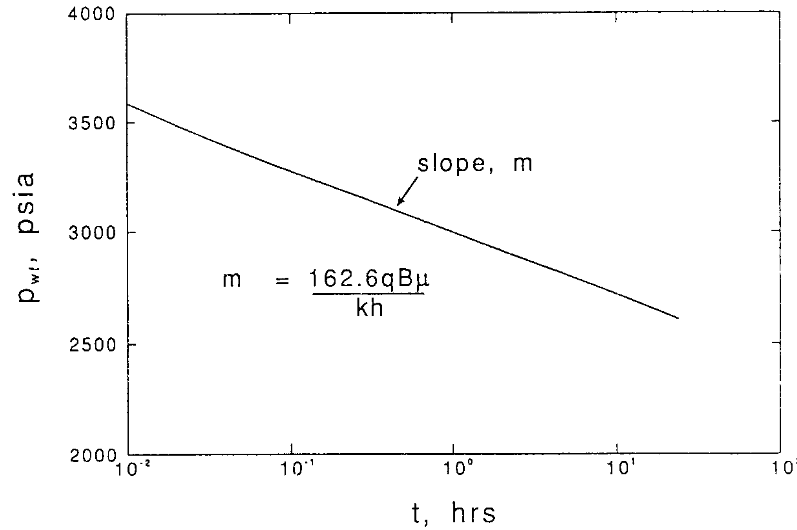

Figure 2 - Infinite-acting, constant rate pressure drawdown behavior

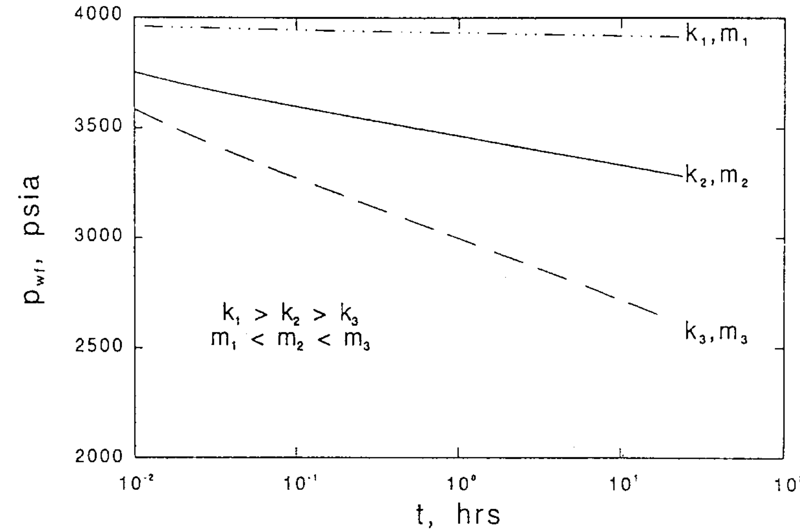

Figure 3 - Drawdown behavior for different permeabilities

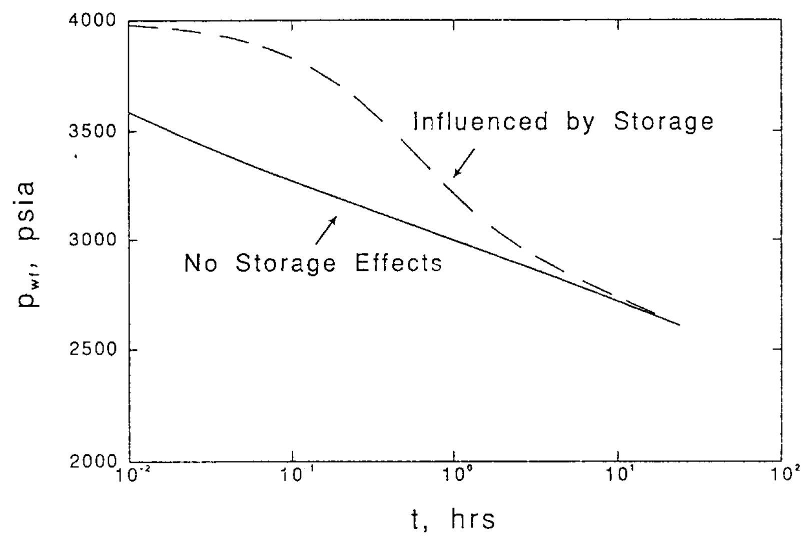

Figure 4 - Effect of wellbore storage on drawdown behavior

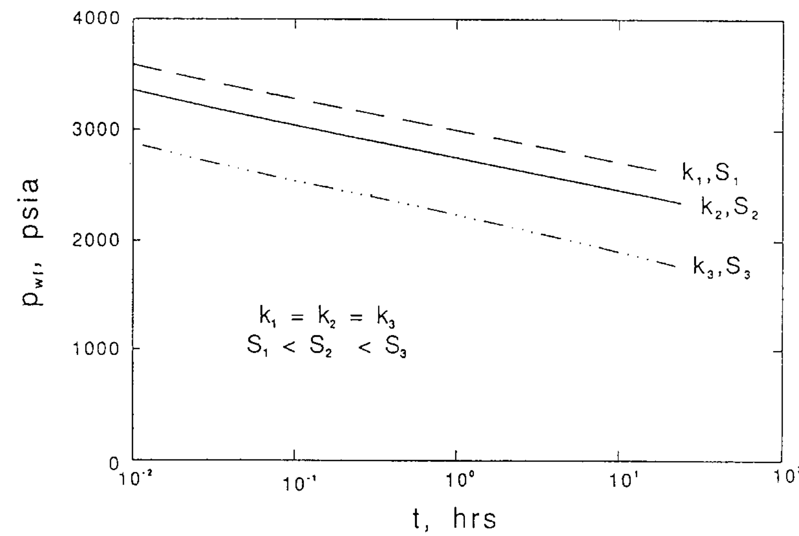

Figure 5 - Drawdown behavior for different skin factors

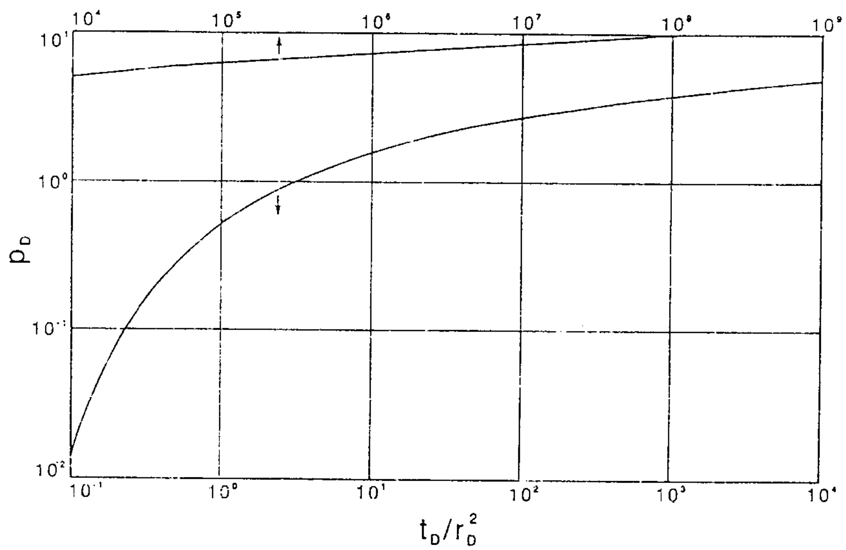

Figure 6 - Exponential-integral solution type curve

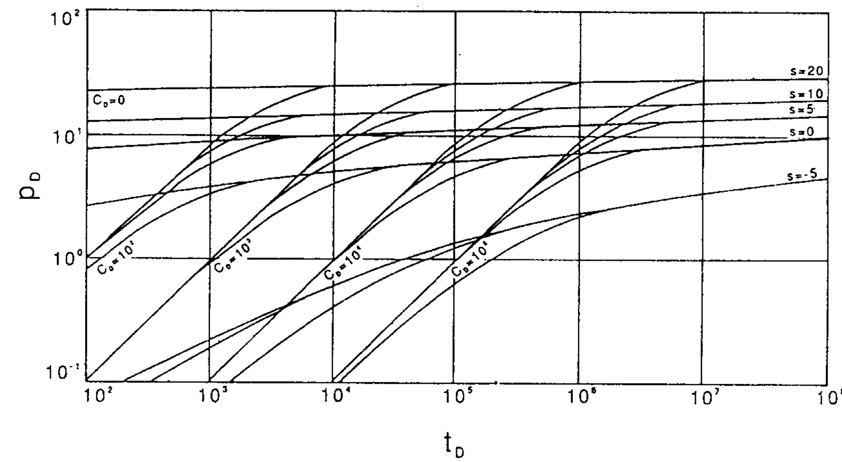

Figure 7 - Ramey type curve

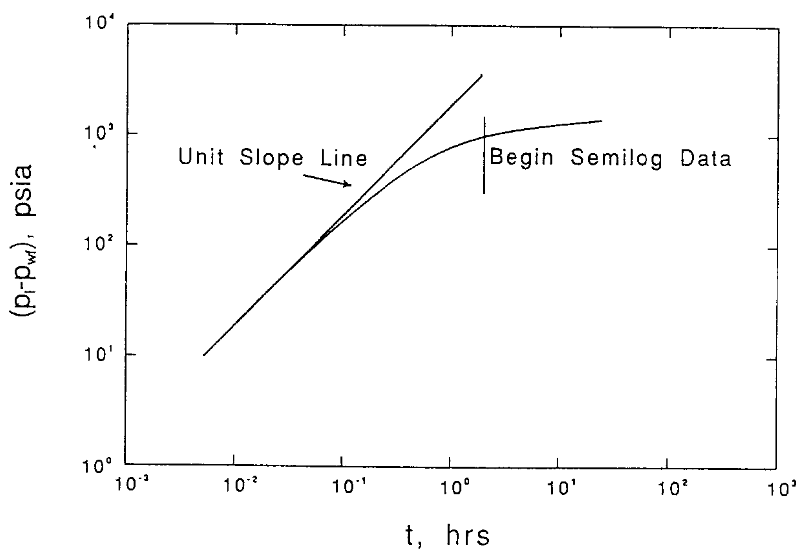

Figure 8 - Log-log plot for storage diagnosis

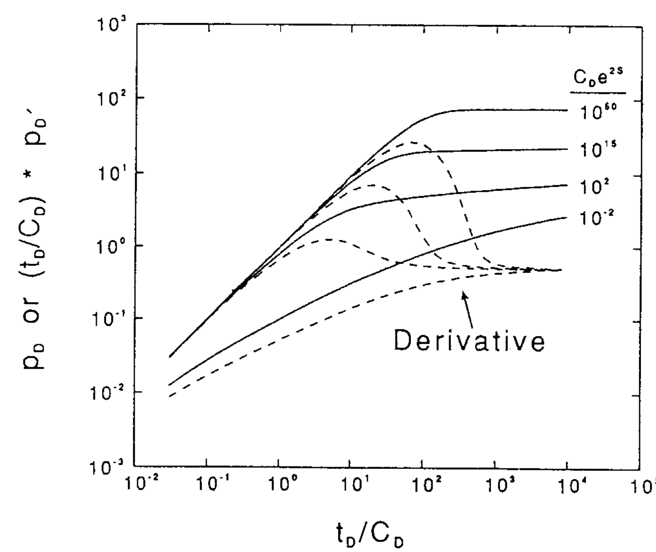

Figure 9 - Radial flow type curve with derivative

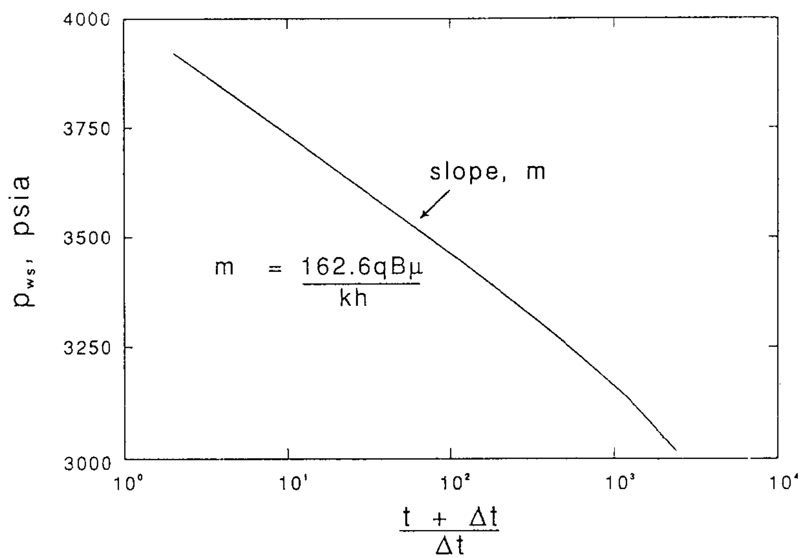

Figure 10 - Infinite-acting pressure buildup behavior

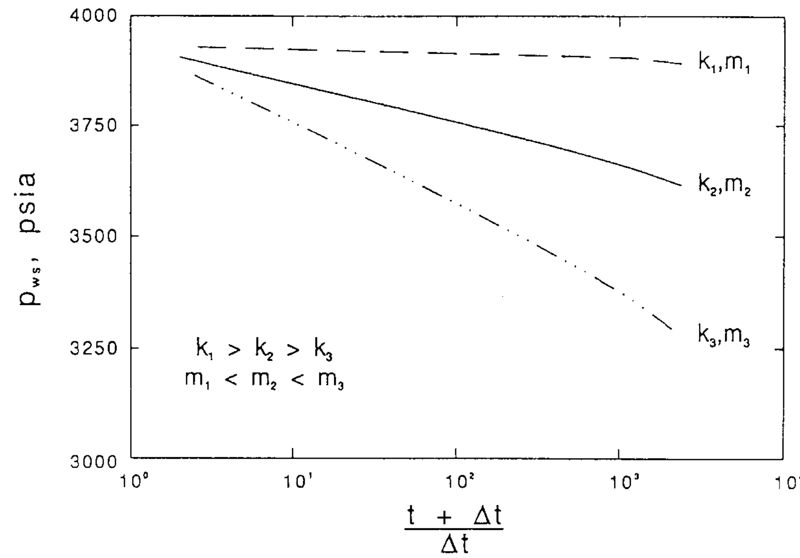

Figure 11 - Buildup behavior for different permeabilities

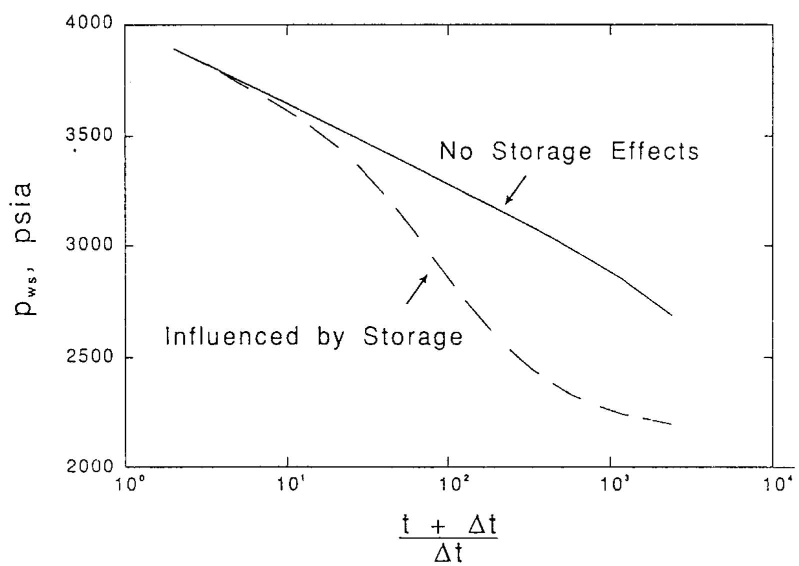

Figure 12 - Effect of wellbore storage on buildup behavior

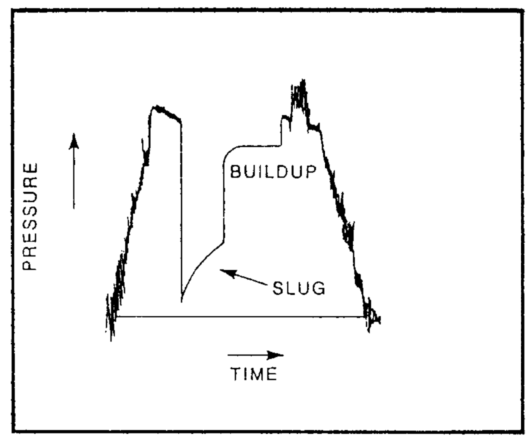

Figure 13 - Typical DST pressure response

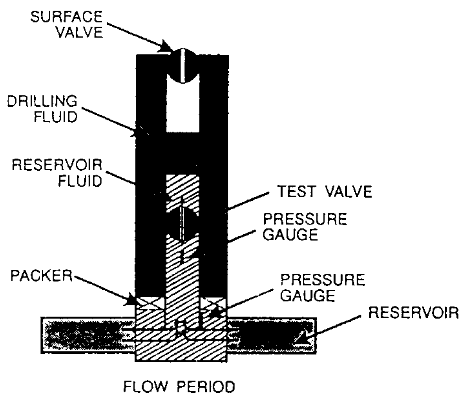

Figure 14 - DST well configuration

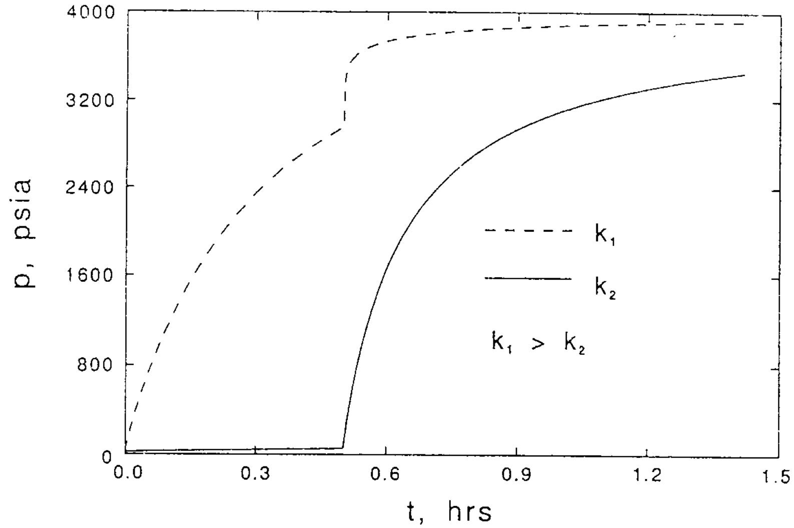

Figure 15 - Effect of permeability on DST behavior

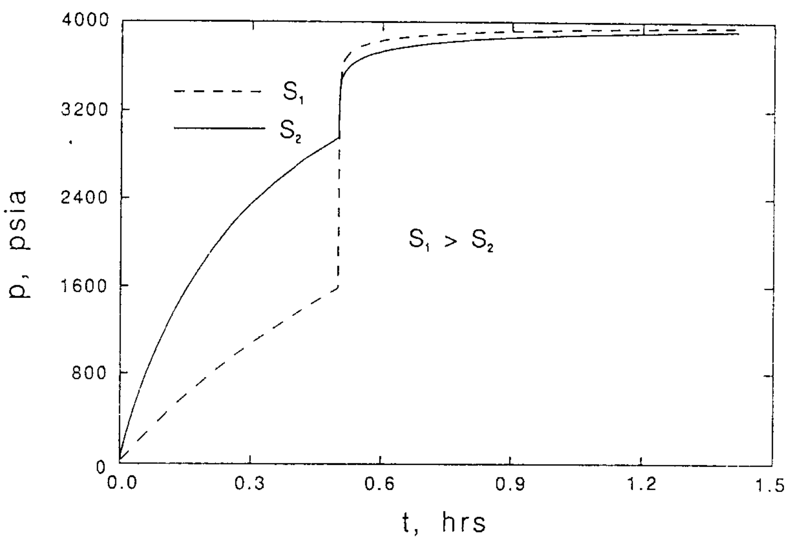

Figure 16 - Effect of skin on high permeability DST behavior

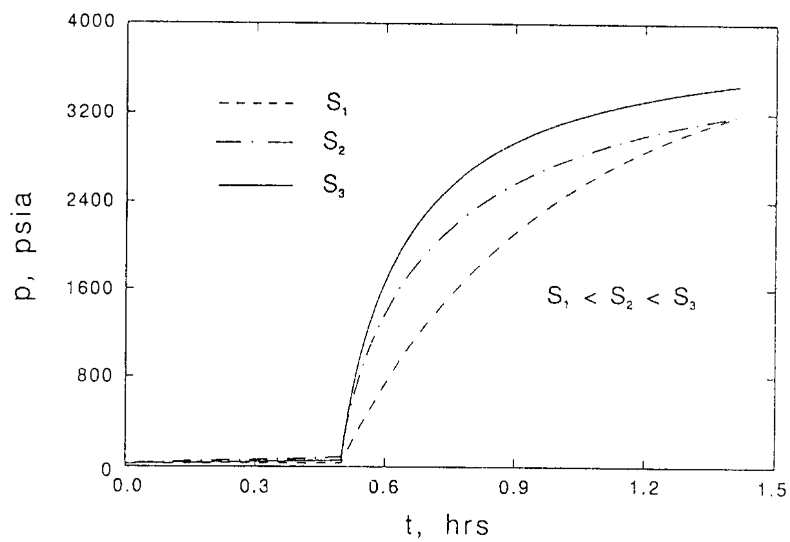

Figure 17 - Effect of skin on low permeability DST behavior

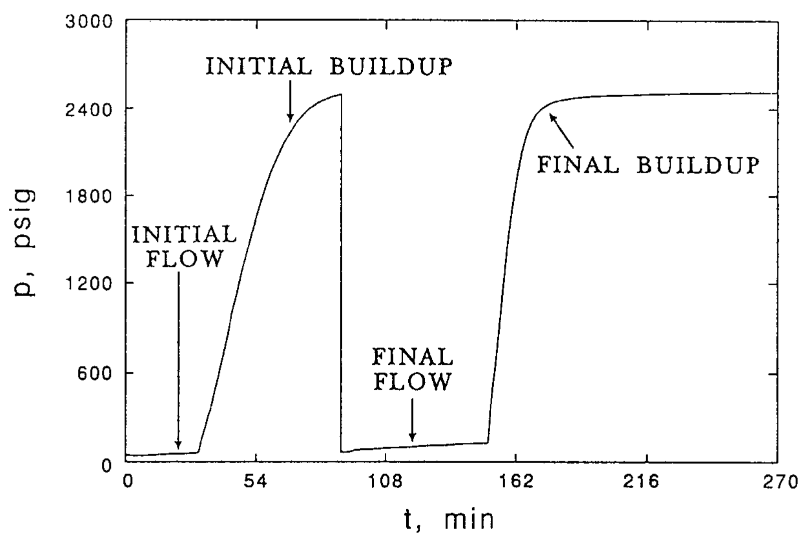

Figure 18 - Oil DST field case - bottomhole pressure

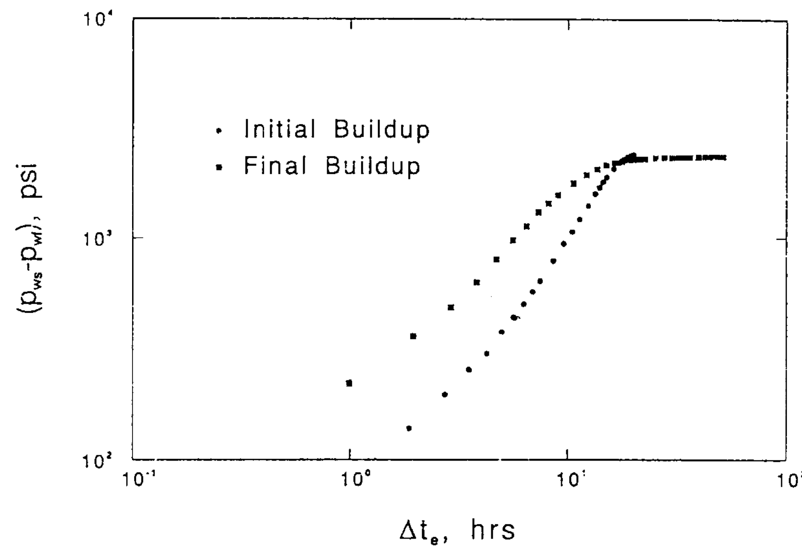

Figure 19 - Oil DST field case - log-log diagnostic plot

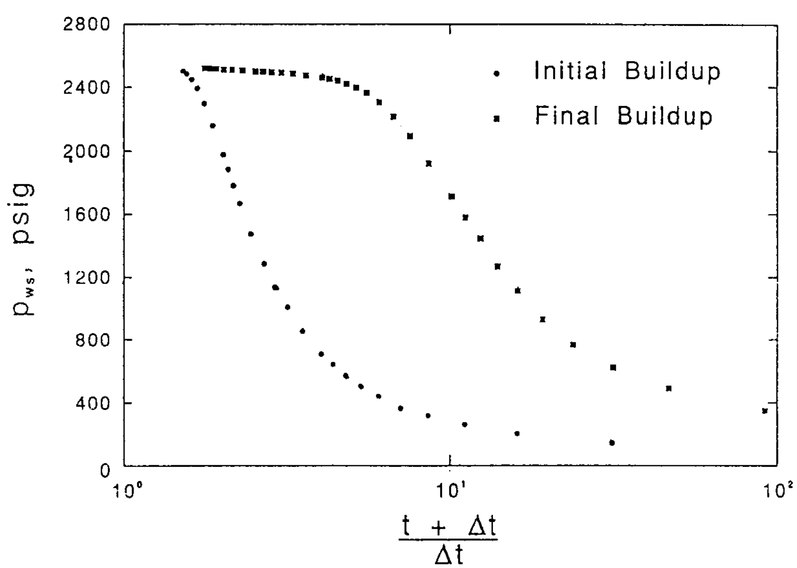

Figure 20 - Oil DST field case - Horner plot

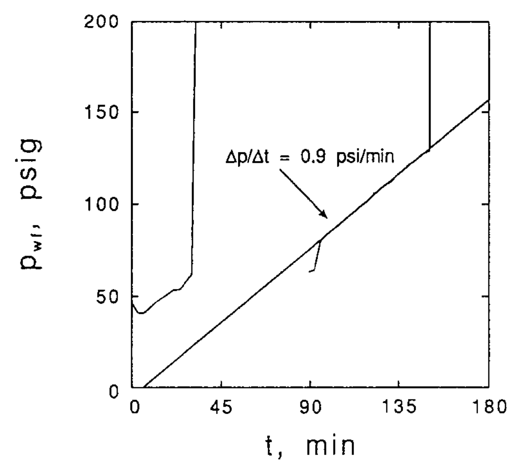

Figure 21 - Oil DST field case - flowing pressures

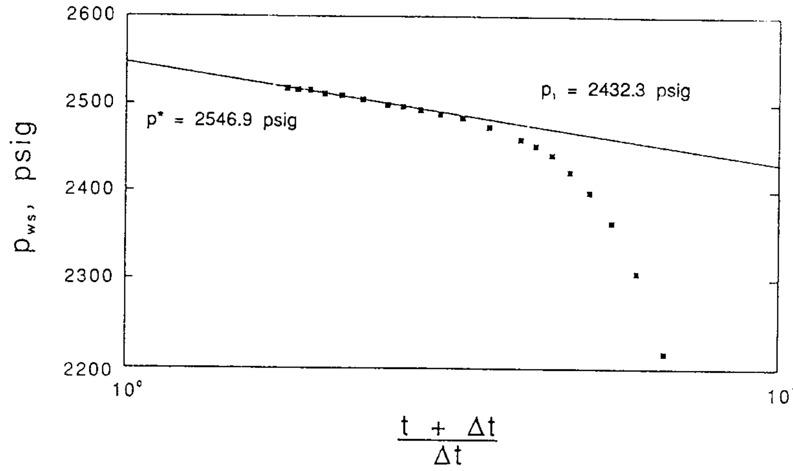

Figure 22 - Oil DST field case - Horner plot of final buildup

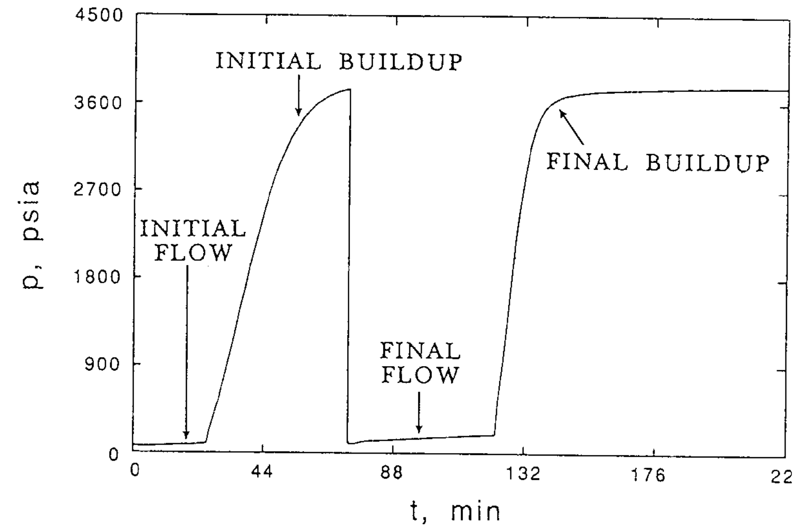

Figure 23 - Gas DST field case - bottomhole pressure

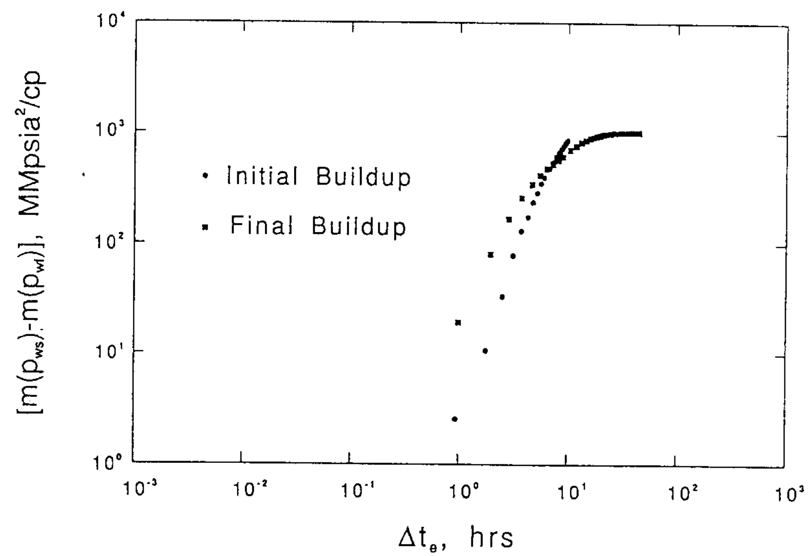

Figure 24 - Gas DST field case - log-log diagnostic plot

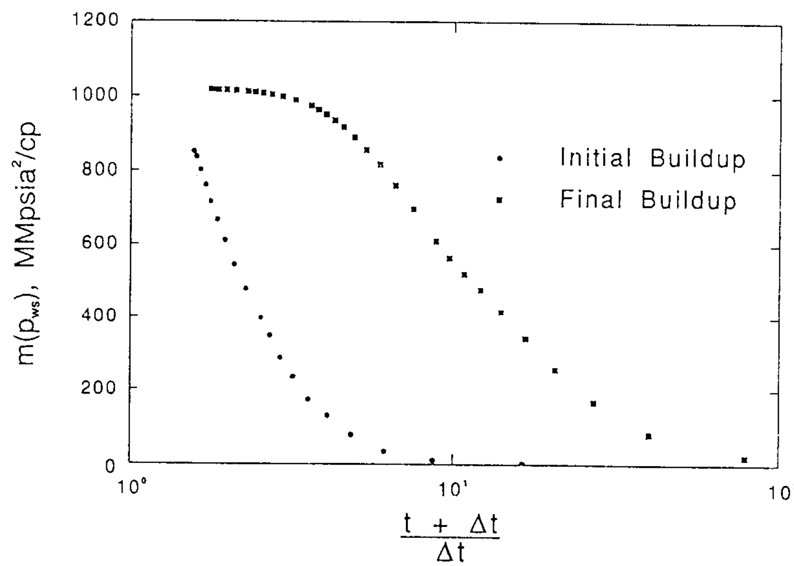

Figure 25 - Gas DST field case - Horner plot

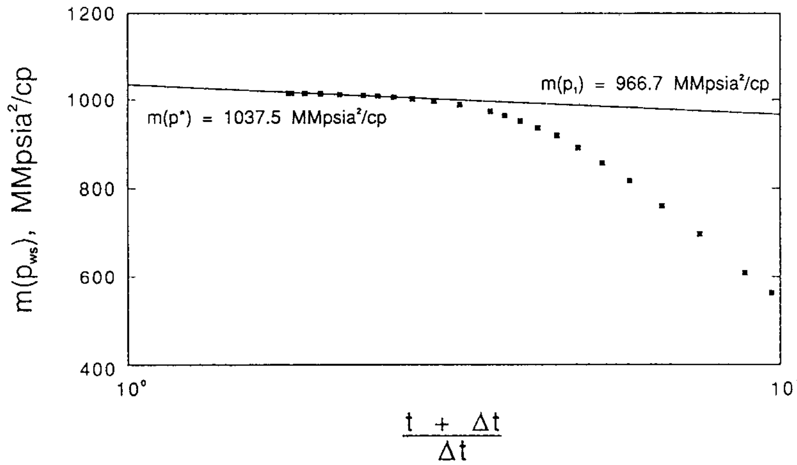

Figure 26 - Gas DST field case - Horner plot of final buildup

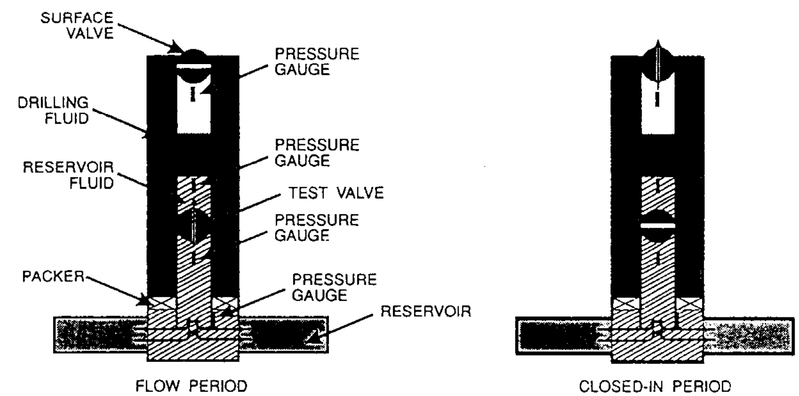

Figure 27 - CCDST well configuration

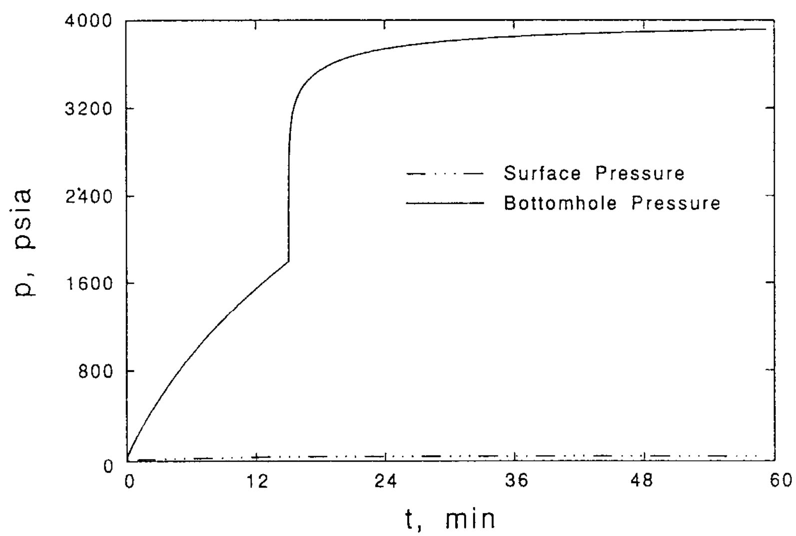

Figure 28 - CCDST behavior - high permeability liquid case

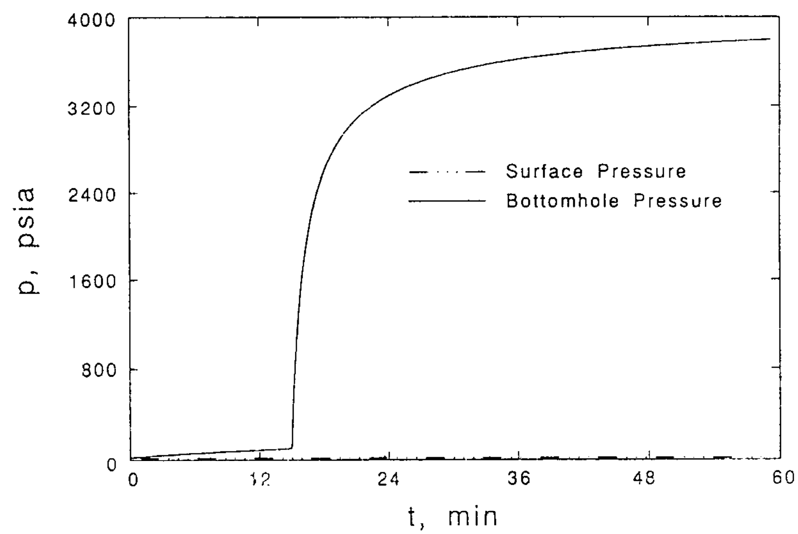

Figure 29 - CCDST behavior - low permeability liquid case

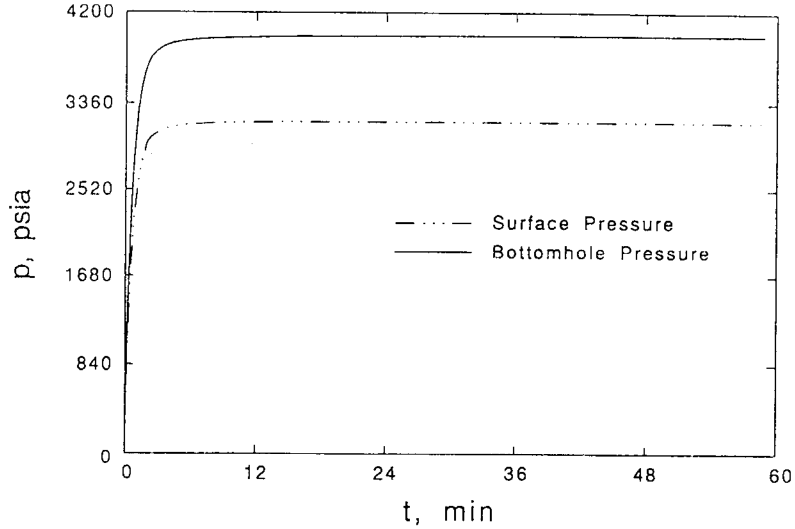

Figure 30 - CCDST behavior - high permeability gas case

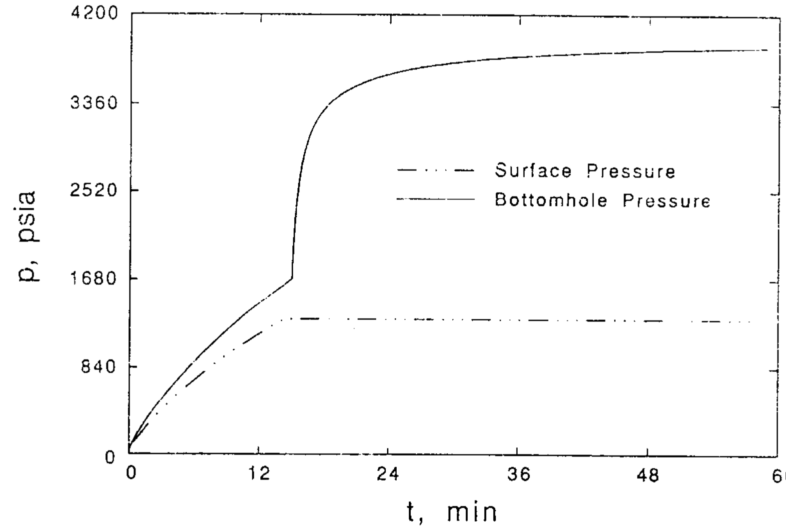

Figure 31 - CCDST behavior - medium permeability gas case

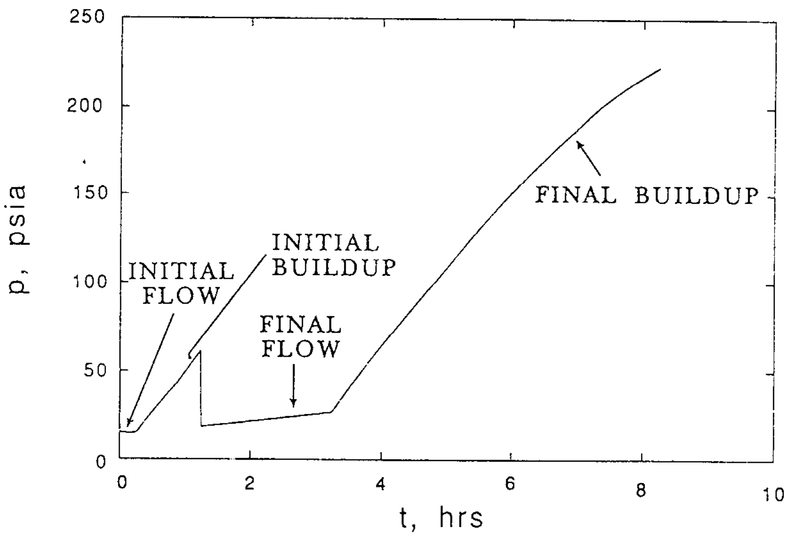

Figure 32 - CCDST field case - bottomhole pressure response

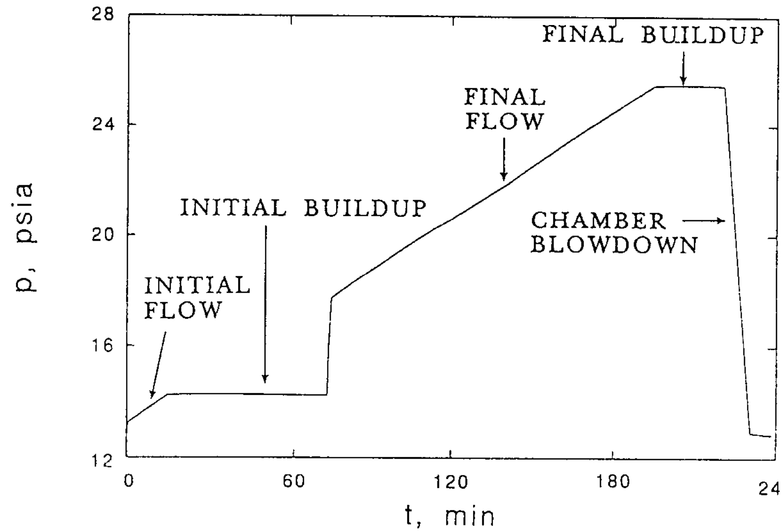

Figure 33 - CCDST field case - surface pressure response

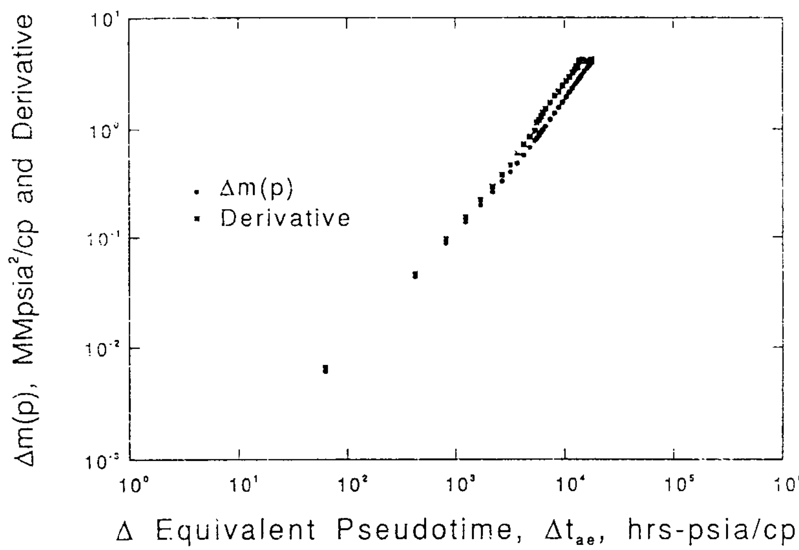

Figure 34 - CCDST field case - derivative log-log plot

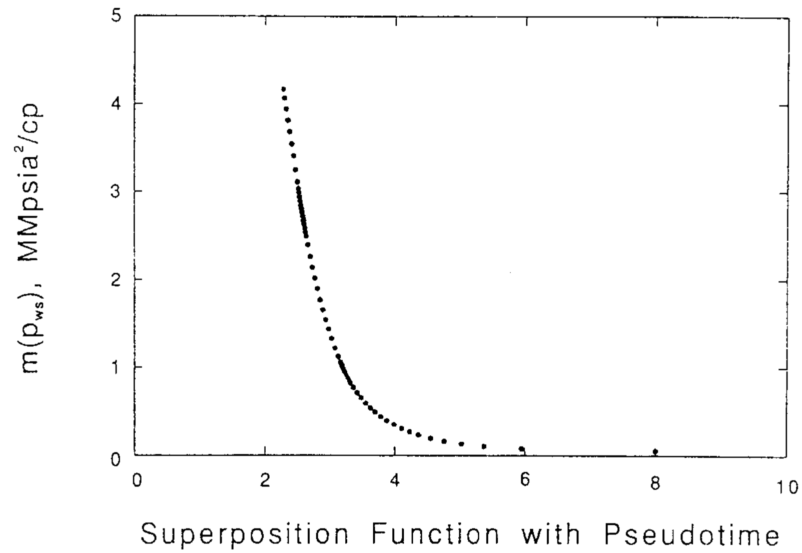

Figure 35 - CCDST field case - superposition plot

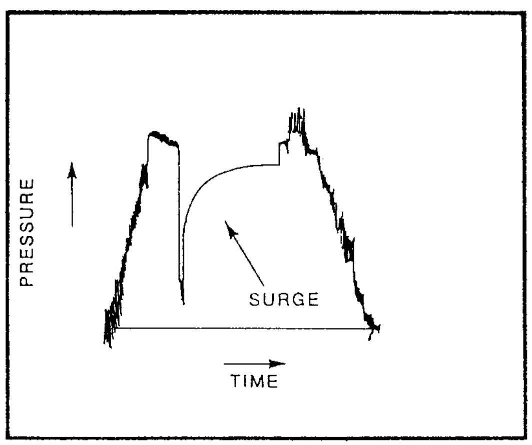

Figure 36 - Typical surge-test pressure response

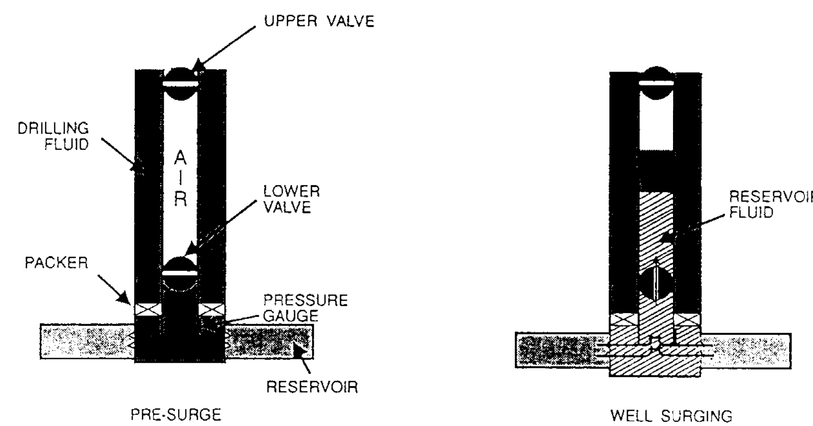

Figure 37 - Surge test well configuration

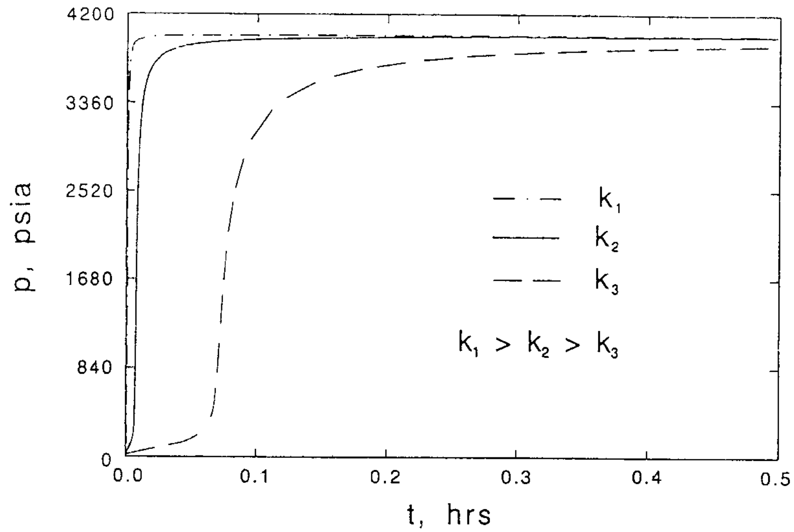

Figure 38 - Effect of permeability on surge behavior

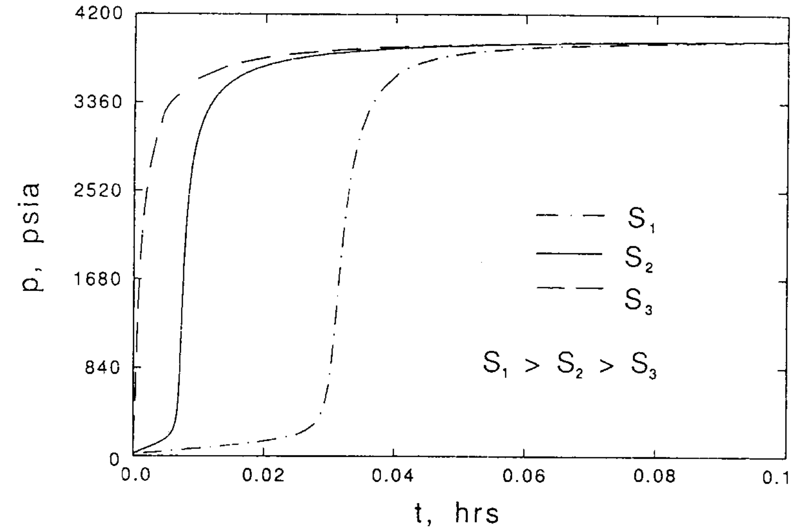

Figure 39 - Effect of skin on surge behavior

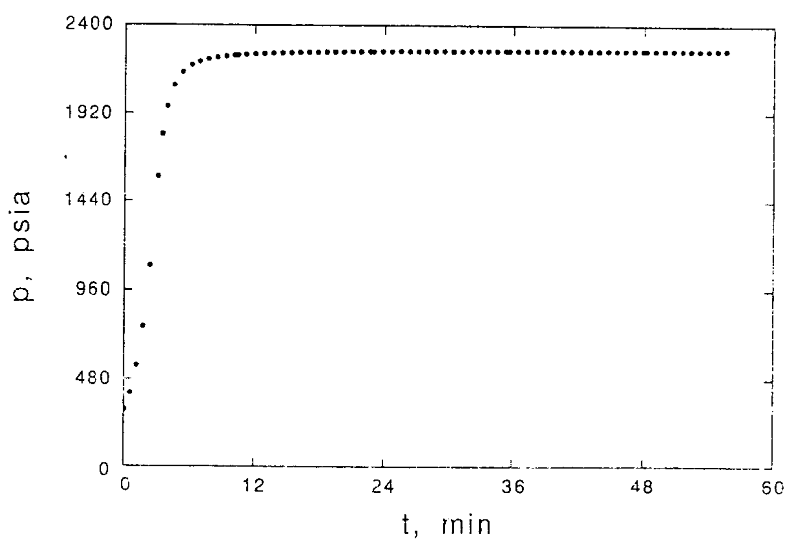

Figure 40 - Surge test field case - pressure response

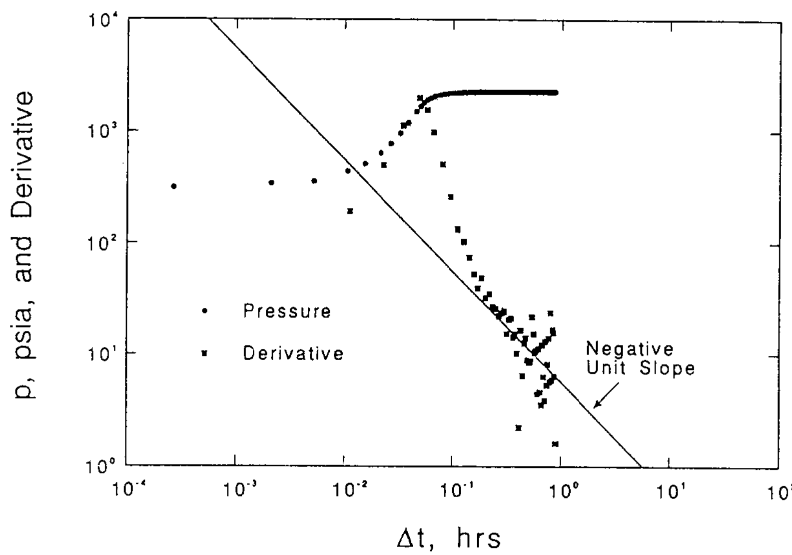

Figure 41 - Surge test field case - derivative log-log plot

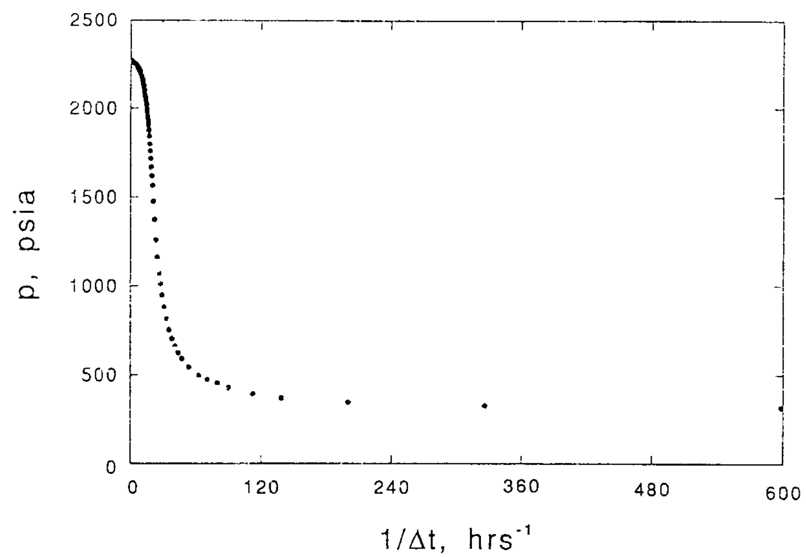

Figure 42 - Surge test field case - linear plot

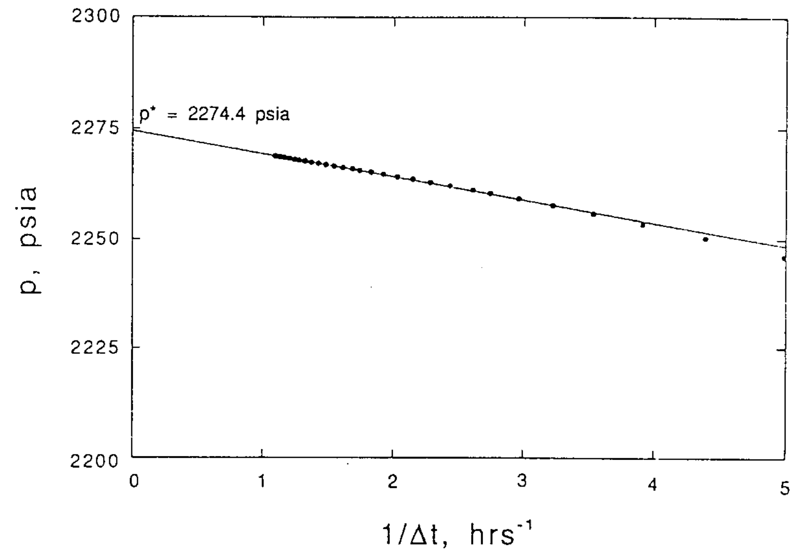

Figure 43 - Surge test field case - late-time expansion of linear plot

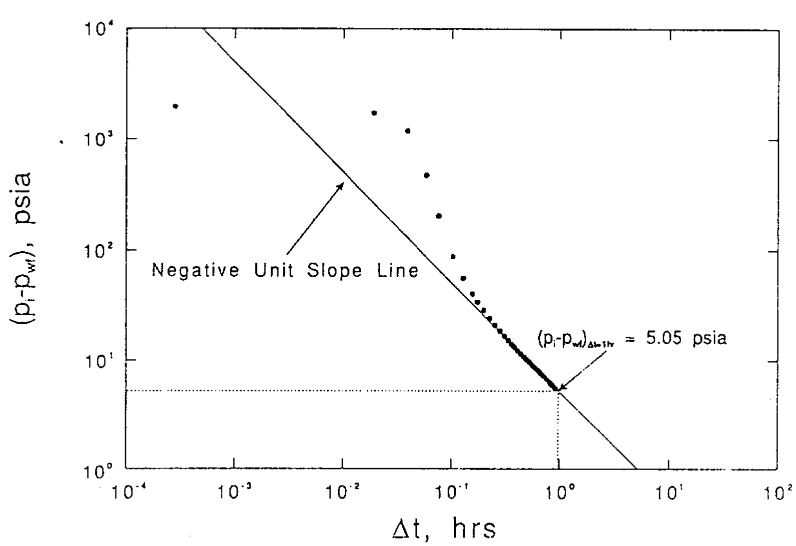

Figure 44 - Surge test field case - log-log analysis plot

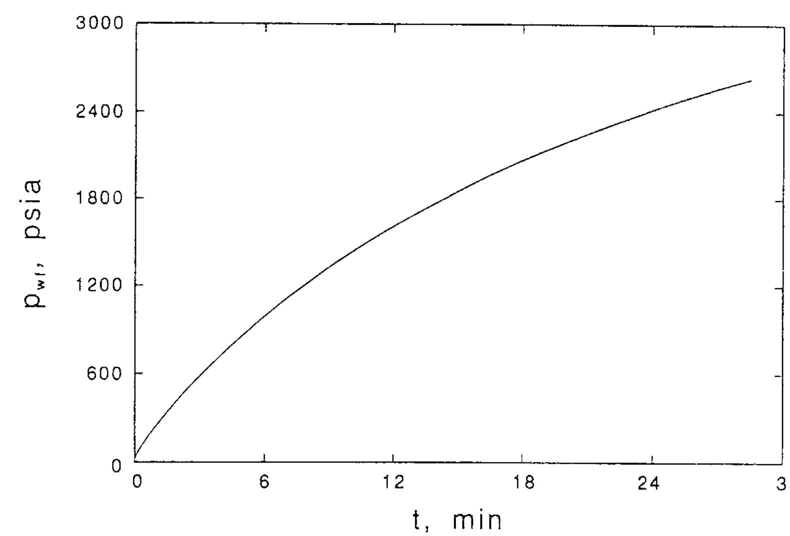

Figure 45 - Slug behavior - subcritical flow

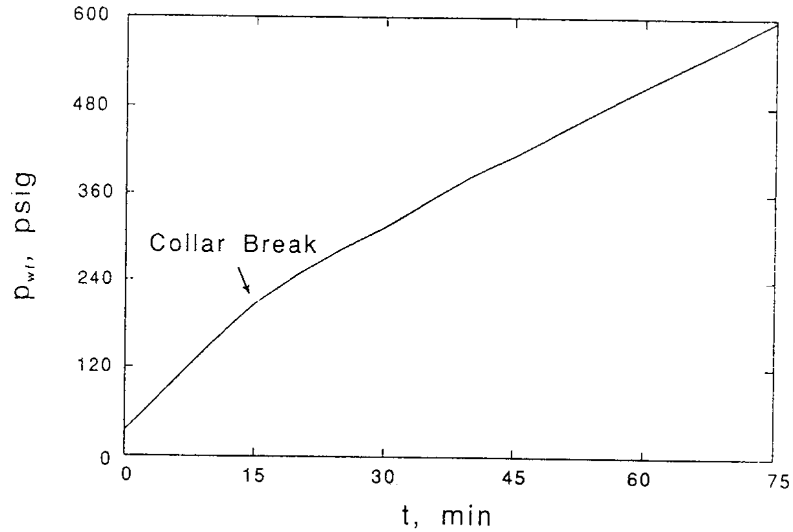

Figure 46 - Slug behavior - critical flow

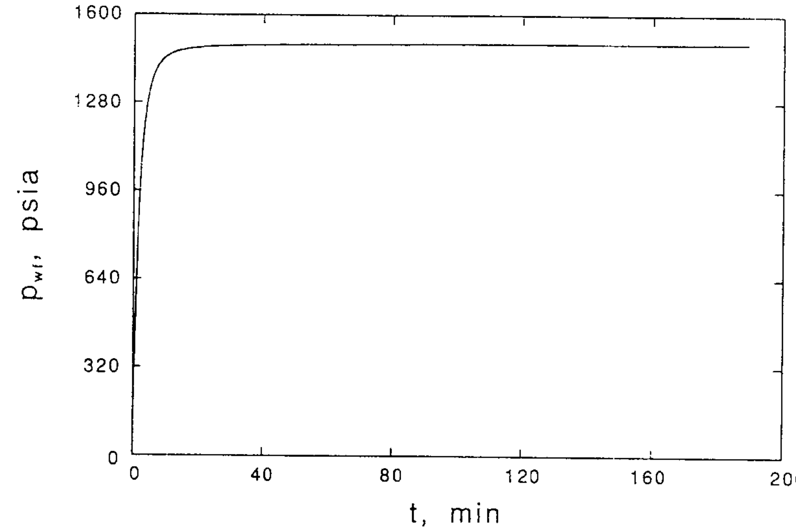

Figure 47 - Slug behavior approximating surge behavior

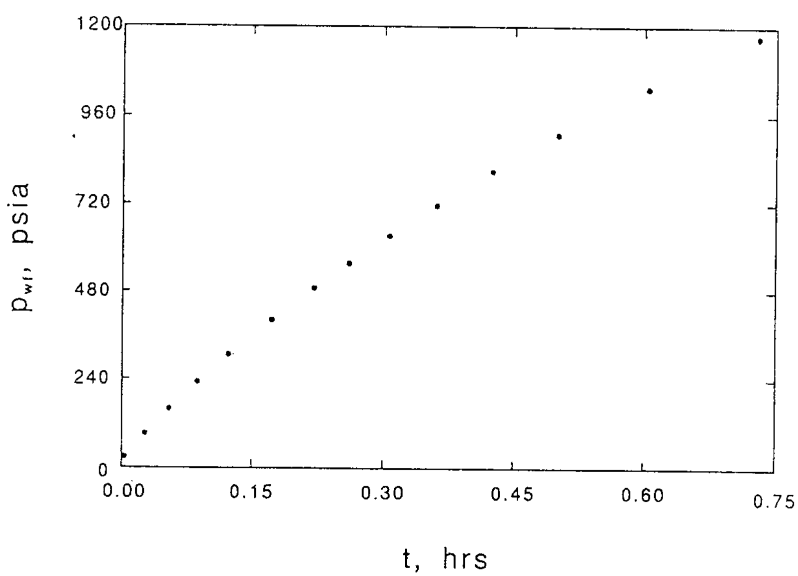

Figure 48 - Simulated slug test

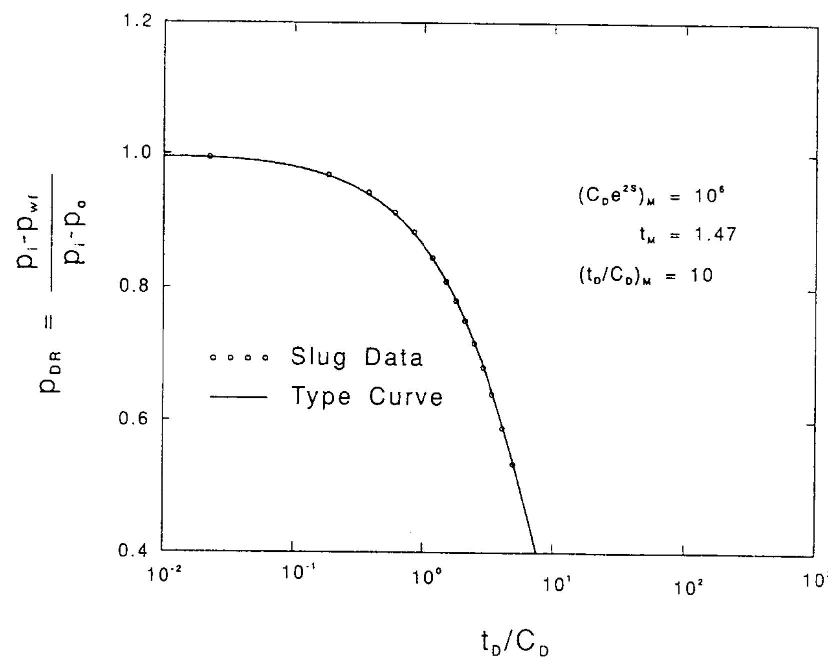

Figure 49 - Slug test - type curve match